A ROBUST SIMULATION-OPTIMIZATION APPROACH FOR DESIGNING HYBRID RENEWABLE ENERGY SYSTEMS

by

Pardis Pourmohammadi

Submitted in partial fulfillment of the
requirements for the degree of

MASTER OF APPLIED SCIENCE

at

DALHOUSIE UNIVERSITY

Halifax, Nova Scotia October , 2021

© Copyright by Pardis Pourmohammadi, 2021

To my wonderful loving family,
for all their support and
dedication.

Table of Contents

List of Tables . . . . . **v**

List of Figures . . . . . **vi**

Abstract . . . . . **vii**

Acknowledgements . . . . . **ix**

Chapter 1 Introduction **1**

Chapter 2 Literature Review **5**

2.1 Model-based Methods 6
2.1.1 Heuristic Methods 6
2.1.2 Commercial Solvers 8

2.2 Metamodel-based Methods 9
2.2.1 Response Surface Methodology 9

2.3 Distributionally-Robust Optimization (DRO) 11

Chapter 3 Problem description and modelling **14**

3.1 Operational Rules 14

3.2 Stochastic supply model 20

3.3 Phi-divergence ambiguity set 21

Chapter 4 Solution Methodology **24**

4.1 Classical Response Surface Methodology 24

4.2 Global Response Surface Technique (GRST) 32

Chapter 5 Case study and results **37**

5.1 Generation of Supply Scenarios 38

5.2 Classical RSM Results 42

5.3 GRST Results 51

Chapter 6 Conclusions and future extensions **58**

Bibliography **61**

List of Tables

2.1	Summary of published studies for optimization of HRES	10
3.1	Common choice of ϕ-divergence	22
4.1	A fractional factorial design for four factors	26
5.1	Model parameters	38
5.2	Number of members and probabilities of clusters	41
5.3	Factors and Levels for R-III	42
5.4	Factors and Levels for CCD	42
5.5	Optimal results for each scenario with $ 40/kWh penalty value	43
5.6	Optimal results for each scenario with $20/kWh penalty value .	44
5.7	Optimal results for each scenario with $10/kWh penalty value .	45
5.8	Nominal problem optimal cost and configuration	45
5.9	Robust problem optimal cost and configuration	47
5.10	TAC for 10 independent realizations with two $\rho = 0$ and $\rho = 0.01$, and their differences	48
5.11	Optimal results for each scenario with $40/kWh penalty value .	51
5.12	Optimal results for each scenario with $20/kWh penalty value .	52
5.13	Optimal results for each scenario with $10/kWh penalty value .	53
5.14	Nominal problem optimal cost and configuration	53
5.15	Robust problem optimal cost and configuration	55
5.16	TAC for 10 independent realizations with two $\rho = 0$ and $\rho = 0.01$, and their differences	55

List of Figures

2.1	A classification of simulation optimization approached	5
3.1	Utilization priority of system resources	16
4.1	A fractional-factorial two-level design for three variables	26
4.2	Central Composite Design for three variables	28
4.3	A flowchart of the Classical RSM	30
4.4	A flowchart of GRST	35
5.1	Northwestern Ontario	37
5.2	Variance of within-cluster sums of point-to-centroid distances	39
5.3	24-element supply power centroid extracted from the time-series data	40
5.4	Generated annual supply power output	40
5.5	Classical RSM: Sensitivity analysis on ρ	46
5.6	Classical RSM: QQ Plot for Z_j	49
5.7	Classical RSM: Pareto frontier for TAC vs reliability	50
5.8	GRST: Sensitivity analysis on ρ	54
5.9	GRST: QQ Plot for Z_j	56
5.10	GRST: Pareto frontier for TAC vs reliability	57

Abstract

Stand-alone hybrid renewable energy systems (HRES) provide a viable alternative to satisfy the energy demand of remote and isolated communities. We consider a PV/Wind/Diesel/Battery HRES and propose a design approach that minimizes the total setup and operations cost and maximizes the supply reliability. A finite number of supply scenarios, extracted from a limited sample of data points through clustering, are first used under the assumption that their probabilities are known with certainty to solve the nominal problem. Next, the robust problem is considered by constructing an ambiguity set, based on the Variation Distance phi-divergence, around the nominal probability distribution and minimizing the expected cost, where the expectation is taken with respect to the worst distribution in the ambiguity set. Since the cost and the reliability functions cannot be evaluated explicitly, they are estimated through simulation based on certain operational rules and using solar and wind supply scenarios drawn at random according to the considered probability distribution (nominal or worst-case). To solve the problem, two novel robust simulation-optimization approaches that estimate a surrogate objective function through a classical Response Surface Methodology (RSM) and a Global Response Surface Technique (GRST) are proposed. The classical RSM approach uses a three-level (R-III) fractional factorial design to estimate the steepest descent direction and perform a gradient search, before using a Central Composite Design (CCD) to estimate a local quadratic approximation and find the optimum solution when the gradient becomes sufficiently small. The GRST, on the other hand, approximates the response function over the entire search space using a convex quadratic function and finds the optimizer of the surrogate function, before restricting the search space around it to obtain a better quadratic approximation and repeat the process. The results obtained from implementing the proposed approaches on a hypothetical case study confirm their applicability and show that the robust solutions outperform those obtained from classical risk-neutral methods when applied with external data samples.

LIST OF ABBREVIATIONS USED

ABC Artificial Bee Colony

CCD Central Composite Design

DRO Distributionally-Robust Optimization

EIR Energy Index Ratio

GHG Green House Gas

$GRST$ Global Response Surface Technique

$HRES$ Hybrid Renewable Energy Systems

LCE Levelized Cost of Energy

LLP Loss of Load Probability

$LPSP$ Loss of Power Supply Probability

NPC Net Present Cost

$QMOO$ Queuing multi-objective optimizer

$R-III$ Resolution-III

RSM Response Surface Methodology

SO Simulation Optimziation

TAC Total Annual Cost

Acknowledgements

I would like to express my sincere gratitude towards people who made accomplishing this dissertation possible. I am thankful to my Supervisor, Dr. Ahmed Saif, for his great support and guidance throughout my Master's studies.

My appreciation extends to my Supervisory Committee Members, Dr. John Blake and Dr. Lei Liu for their time, discussions, and beneficial comments on my research project. I am also grateful to Dr. Peter Vanberkel for accepting to be my Defense Moderator.

I would like to gratefully acknowledge the financial support from Nova Scotia Graduate Scholarships Support Research, through the Nova Scotia Graduate Scholarship program (NSGS).

Finally, I am genuinely thankful to my beloved parents and my best friends who have always been there for me with their patience, love, and support.

Chapter 1

Introduction

With the growth in agricultural, industrial, and domestic activities, energy demand is rapidly growing all around the world. This has meant the depletion of fossil fuels, which is the main driving force behind the efforts to utilize renewable energy sources more effectively [1]. Other reasons like the techno-economic advantages of renewable energy combinations, the growing interest in sustainability and the desire to decrease GHG emissions, have made them a viable alternative to conventional sources [2]. Renewable energy is a multidisciplinary area, and nowadays, people from different fields are bringing in a broad range of expertise to increase the utilization of renewable energy resources.

Hybrid renewable energy systems (HRES) combine two or more locally available renewable energy resources such as wind, solar, biomass, and small hydro power, together with or without conventional sources. They are particularly viable when the costs of connection to the long-distance transmission or distribution grid are too high. Thus, they operate in a standalone mode to meet the energy needs in rural remote areas. Combining these renewable energy sources with back-up units can provide a more reliable supply of electricity in all load demand conditions compared to the single-use of such systems [3]. The cost, supply reliability, and environmental impact, among other metrics, of HRES depend on the type, size, location and operational strategy of the system components. Hence, the topic of designing HRES has attracted a considerable attention in the last few decades, and several methods have been proposed for this purpose. Since wind and solar are among the most widely available renewable energy resources, several studies have focused on designing HRES consisting of Photo-voltaic (PV) panels and Wind Turbines, combined with conventional generators, e.g., diesel generators, and energy storage, e.g., batteries, to serve the demand reliably, efficiently and in an eco-friendly fashion [4, 5, 6, 7, 8].

Several technical and economic criteria must be considered when designing HRES.

These criteria include delivering energy at optimum efficiency, GHG emissions targets and limits, and the ability to fulfill the load demand with high reliability [2]. Power reliability analysis is considered a major step in the system design process. Multiple reliability indices have been proposed in the literature. Among the most widely-used indices are the Loss of Power Supply Probability (LPSP) and the Loss of Load Probability (LLP), both illustrate the inability of the HRES to meet the demand load [9]. LPSP, defined as the number of times power supply was unable to meet the demand (during certain interval) over the total number of times a power supply is exploited, is considered as a constraint in [10, 11, 12, 13, 14], whereas LLP is used as a reliability objective where unmet demand is divided by the total demand load and is minimized in [15, 16, 17, 18, 19].

Moreover, cost is another primary design criterion for HRES. Renewable energy systems generally entail high capital costs, even though they have low operation and maintenance (O&M) costs. An economic and break-even analysis is required to determine the optimum cost to achieve the least possible unit price of the HRES [3]. Several metrics have been developed to quantify the economic performance of HRES, including the levelized cost of energy (LCE), the net present cost (NPC), the total life cycle cost (LCC), and the annualized cost of the system (ACS). Intuitively, minimizing cost and maximizing reliability are two conflicting objectives, since additional costly energy generation and storage capacities are needed to increase reliability. Therefore, the aim is to find the best trade-off between these contradictory objectives. There are plenty of studies in the literature that aim at minimizing cost and maximizing reliability in standalone HRES such as [4, 20, 21, 13, 14]. However, to the best of our knowledge, none of these studies considered the uncertainty in probability distribution of supply power.

In this thesis, a robust methodology for designing a standalone HRES is proposed to minimize total annual cost (TAC) while ensuring a pre-defined level of LLP. The proposed approach focuses on implementing and extending a novel, distributionally robust simulation-optimization model that accounts for uncertainty in the probability of supply power data by using an ambiguity set based on phi-divergence. Since the closed-form of the objective function is not available, two response surface metamodels are fitted on input/output simulation data using design of experiments (DoE)

as a surrogate function. The first approach, referred to as the classical RSM, fits a first-order polynomial in the neighborhood of the starting point to find the steepest descent direction. After several steps moving towards the direction, it gets close to the neighborhood of the optimum (where the gradient becomes small). Then, a quadratic function is fit on this neighborhood to find the optimum solution. The second approach, referred to as the GRST, fits a convex quadratic function on the entire search space and reduces the search space in subsequent iterations to the neighborhood of the best solution found so far. Finally, the proposed methods are implemented on a hypothetical case study in Ontario. In this study:

- A k-means clustering approach is applied to effectively use the available limited time-series data in order to extract a manageable number of supply scenarios and estimate their probability of occurrence from the historical data.

- Two metamodel approaches, namely classical RSM and GRST, are combined for the first time with distributionally-robust optimization (DRO) to handle the dual issue of the lack of explicit objective functional form and uncertainty about the probability distribution of the supply scenarios by allowing these probabilities to be perturbed within an ambiguity set to account for estimation errors.

- An ambiguity set is build based on the Variation Distance phi-divergence, and the proposed metamodels methods are implemented and solved on a hypothetical case study for two problems: the nominal (when the probabilities of scenarios are deterministic) and robust (when probabilities are uncertain) problem.

The remainder of this thesis is organized as follows: in Chapter 2, a brief review of the literature related on the application of simulation optimization methods to design HRES is presented. Chapter 3 emphasizes on the simulation, problem modelling and its operational rules. Generating scenarios for the stochastic power supply using a k-means clustering approach and a basic concept of phi-divergence are also explained in this section. Chapter 4 explains, in detail, the two approaches proposed to robustly design a HRES: the classical RSM and the GRST. The regression models used to fit the input/output data in each approach are presented, along with the way

distributional ambiguity is incorporated into the design process. In Chapter 5, the proposed methods are applied to a case study in northwest Ontario, Canada. First, supply scenarios are generated, then, the results obtained from the two proposed methods are presented and compared. Finally, Chapter 6 provides the conclusion and ideas for future research.

Chapter 2

Literature Review

A widely-used modern optimization approach which is particularly useful when the objective function cannot be expressed analytically is Simulation Optimization (SO) [22]. SO is the process of finding the best input variable values from all possibilities without evaluating each of them explicitly [23]. As opposed to algebraic model-based mathematical programming, SO does not assume that an algebraic description of the simulation is available. The simulation may be treated as a black box that only allows evaluating the objective and constraints for a particular input [23]. In fact, many SO algorithmic approaches solely depend on such input-output data from the simulation in their search for optimal input settings. This domain (SO) includes various methodologies, as it is briefly depicted in Figure 2.1 [23].

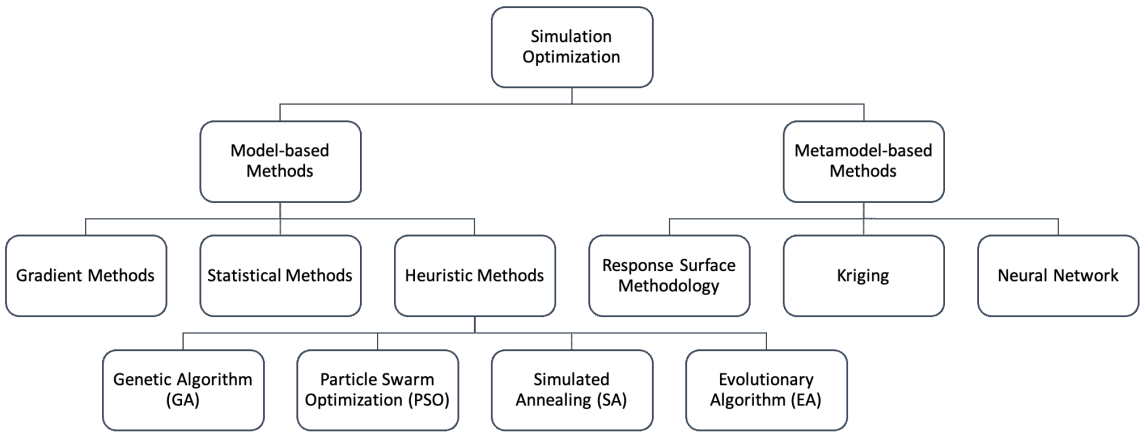

Figure 2.1: A classification of simulation optimization approached

SO methods can be categorized into model-based and metamodel-based methods. Model-based methods include heuristic methods (GA, PSO, SA,...), gradient

methods (Finite Difference Estimation, Likelihood Ratio Estimator (LR), Perturbation Analysis (PA)), statistical methods (Importance Sampling, Rank and Selection, Multiple Comparison) and commercial solvers (HOMER [24], iHOGA [25], OptQuest [26],...)[23]. Although software programs are not specific methods by themselves, they are programmed to solve the problem based on certain search/optimization methods. The next subsections review some representative examples of these methods in the domain of HRES design.

2.1 Model-based Methods

Amongst all model-based simulation optimization methodologies, heuristic methods and commercial solvers are the most-applied approaches/tools in optimizing HRES problems. In the following subsections, representative examples from the literature of model-based SO for designing HRES are reviewed.

2.1.1 Heuristic Methods

Heuristic methods are commonly used for HRES optimization due to the non-linear behaviour of some of the variables involved [27]. Many of these techniques balance exploration with exploitation, thereby resulting in efficient global search strategies. Among the methods for optimizing HRES GA, PSO, and SA are the most commonly used algorithms for sizing HRES [28]. The heuristic methods discussed below represent the developments in the field of direct search methods (requiring only function values) that are frequently used for simulation optimization with a special focus on the renewable energy system application.

- **Genetic Algorithm (GA)**

  The GA is a stochastic global search method that imitates the natural biological evolution metaphor. It is important to note that GA provides a number of potential solutions to a given problem and the choice of the final solution is left to the user [13]. This algorithm is suitable for optimizing engineering energy systems, which are generally non-linear, and uses a statistical technique of grouping the individual based on a independent variable. It was applied in [21], [27], [18], [6], [13], [14] and [29] to find the optimal design of

HRES, GA can also be implemented on problems with more than one objective. A Multi-Objective Genetic Algorithm (MOGA), commonly referred to as the Non-Dominated Sorting Genetic Algorithm-II (NSGA-II), is used as an optimization algorithm in [30], [6], [31] to find a set of equally good solutions for the objectives as a form of a Pareto frontier. A Hybrid Optimization by Genetic Algorithm (HOGA) software was used in [32] and [33] to design and optimize both a PV-Diesel system and a Wind-Battery system, respectively.

- **Particle Swarm Optimization (PSO)**

  Inspired initially by flocking birds or fishes, Particle Swarm Optimization (PSO) is another form of evolutionary computation and is stochastic in nature, like Genetic Algorithms. PSO has a set number of particles that move through the different layers of the problem. This algorithm has been shown to have advantages as GA without the big computational hit. Unlike in genetic algorithms and evolutionary strategies, in PSO, there is no selection operation. PSO is implemented as an optimization technique to optimize the HRES in [4, 20, 34, 19]. The energy cost is optimized in [35] using PSO and is compared with genetic algorithm and HOMER software. Another comparative analysis of a proposed PSO methodology with the HOMER software tool is presented in [2] for a case study of various stand-alone HRES arrangement. As a case of more than one objective, Baghaee et al. [36] used MOPSO algorithm to minimize costs of the system and maximize its reliability. A dynamic multi-objective particle swarm optimization (DMOPSO) algorithm, along with a simulation module and a sampling average technique, are used in [37] to approximate a Pareto front (PF) for an HRES design through a multi-objective optimization framework.

- **Simulated Annealing (SA)**

  Simulated annealing is a stochastic search method analogous to the physical annealing process where an alloy is cooled gradually to achieve a minimal energy state. SA avoids getting stuck in local optima (hill-climbing) and keeps track of the best objective value overall. SA performs well on combinatorial problems. Ekren and Ekren [38] performed Simulated Annealing (SA) algorithm, which uses a stochastic gradient search for the global optimization for

optimizing the size of a PV/wind integrated hybrid energy system with battery storage. The optimum result obtained by SA algorithm is compared with former study's result ([17] and [16]). Consequently, it has been shown that the SA algorithm leads to better results than the Response Surface Methodology (RSM). Other studies that implemented SA as an optimization algorithm are reviewed in [1].

- **Evolutionary Algorithms (EA)**

  Similar to GA, evolutionary strategies (ES) are algorithms that mimic the principles of natural evolution as a method to solve parameter optimization problems. Evolutionary Multi-Objective Algorithms (MOEAs) are applied in numerous studies. From the MOEAs that have been developed until now, the Strength Pareto Evolutionary Algorithm (SPEA) is one of the most efficient algorithms. It is applied in [5], for the first time, to the multi-objective design of isolated hybrid systems used for electricity generation. Another evolutionary algorithm is Artificial Bee Colony (ABC). Singh and Kaushik [39] developed an ABC algorithm to detect the optimum hybrid system configuration and performed a comparative analysis between the ABC algorithm and HOMER for cost-effectiveness. Singh et al. [40] also applied an ABC algorithm to provide optimal sizing and scheduling of PV-wind-biomass systems and compared the achieved result with results from PSO algorithm and HOMER. Queuing multi-objective optimizer (QMOO) is another evolutionary algorithm that is used in [41] to optimize the integrated energy systems for remote communities.

2.1.2 Commercial Solvers

Nowadays, optimal and near-optimal solutions for applications are found in minutes instead of performing an exhaustive examination of relevant alternatives in days or months. Simulation programs are not methods per se and they use certain search/optimization methods to find the best solution. OptQuest and HOMER are two prevalent commercial solvers having special search procedures to guide a series of simulations in renewable energy systems. OptQuest integrates simulation, an intelligent search procedure called scatter search (based on Tabu Search), a mixed integer

programming solver, and a method to configure and train neural networks. It can handle multiple objectives and linear constraints on the input variables. In [16] and [42], the OptQuest tool in ARENA software is used to optimize HRES. HOMER, on the other hand, a power optimization software developed by the National Renewable Energy Laboratory, Golden, Colorado, USA, is the most-used optimization software for hybrid systems. It is able to optimize hybrid systems consisting of a PV generator, batteries, wind turbines, hydraulic turbines, AC generators, fuel cells, electrolyzers, hydrogen tanks, AC–DC bidirectional converters, and boilers. It has been used in [22], [43], [40], [44], [39], [45] and [46] as an optimization tool.

2.2 Metamodel-based Methods

Metamodel-based or surrogate models are simpler approximations of the system i.e. models of the model [47]. Due to the complicated nature of HRES and the large number of input variables, metamodels are an intuitive way to tackle the stochastic nature of these systems. Response Surface, Kriging and Neural network methods are amongst the most widely-used metamodels. Ohsawa et al. [48] applied neural networks to the operation control strategies of power PV–Diesel hybrid power generation systems. Mellit et al. [49] investigated the possibility of using an adaptive artificial neural network model for sizing stand-alone photovoltaic systems. Mellit et al. [50] developed an artificial neural network-based genetic algorithm (ANN-GA) model for sizing stand-alone photovoltaic systems.

2.2.1 Response Surface Methodology

Response Surface Methodology (RSM) is a widely used mathematical and statistical method for modeling and analyzing in simulation optimization. Despite the practical use of RSM, the relevant literature is very sparse in the context of HRES. Ekren and Ekren [17] are among the first that used RSM to optimize the sizing of an autonomous PV/wind hybrid energy system with battery storage by minimizing the system cost and loss of load probability. Later, Ekren and Ekren [51] conducted a break-even analysis of the same system with the extension of a transmission line and used the net present value (NPV) to compare both cases. Ren et al. [52] presented

a simulation-based strategy for optimal design of a renewable cooling and heating system. The computational cost of the optimization was significantly reduced by integrating an integer-based genetic algorithm (IGA) with the response surface method (RSM) as compared to the conventional GA. None of these studies have considered the stochastic nature of supply and demand power data. Chang and Lin[53] proposed a RSM-based method, coupled with a Monte Carlo approach for the design of hybrid renewable energy systems in uncertain environments. They considered M power stations and N demand nodes, yet did not acknowledge the probability of uncertain parameters. Along RSM, global response surface techniques are another easy-to-apply metamodels. Sobester et al. [54] and Rais-Rohani et al. [55] investigated the development and applications of global response surface approximation models and proposed a selection criterion which allows relatively precise control of the scope of the search.

Table 2.1 summarizes the main features of the aforementioned HRES studies in terms of their system combination, grid connectivity, objective function and their design optimization.

Authors	System Component						Off-Grid	MOP	Objective Function	Optimization Approach
	PV	WT	DG	Battery	Biomass	Others				
[18]	✓		✓	✓			✓	Yes	TAC, LLP, GHG emission	GA
[21]	✓	✓	✓				✓	Yes	LCE, LPSP	GA
[30]	✓	✓		✓			×	Yes	operation cost, LPSP	NSGA II
[22]	✓	✓			✓		×	No	LCE	HOMER
[33]		✓		✓			✓	No	NPC	HOGA
[43]	✓	✓			✓	✓	✓	Yes	operation cost, EIR	HOMER
[45]	✓	✓	✓				✓	Yes	CO2 emission, operation cost	HOMER
[4]	✓	✓	✓	✓			✓	Yes	LCE, LPSP	PSO
[39]	✓				✓		✓/×	No	TAC, LCE	ABC
[51]	✓	✓		✓			✓	No	NPC	RSM
[41]	✓		✓				✓	Yes	CO2 emission, operation cost	QMOO
[6]	✓	✓	✓	✓			✓	Yes	LCE, CO2 emission	NSGA II
[5]	✓	✓	✓	✓			✓	Yes	CO2 emission, operation cost	SPEA
[37]	✓	✓			✓	✓	×	Yes	NPC, LLP, Co2 emission	PSO
[48]	✓		✓	✓			✓	Yes	operation cost, LPSP	Neural Network

Table 2.1: Summary of published studies for optimization of HRES

2.3 Distributionally-Robust Optimization (DRO)

The intermittent and unpredictable nature of renewable energy sources is a significant challenge, which hinders their use solely as a reliable source of power. Unfortunately, SO methodologies ignore the fact that, in practice, some inputs of the given simulation model are uncertain, so the optimum solution that is derived—ignoring these uncertainties—may be suboptimal [56]. SO models are generally sensitive to the simulation parameters, and to overcome this problem, they need to be hedged against uncertainty. Various robust optimization approaches based on simulated systems were investigated by Dellino [57]. Their proposed methodology uses Taguchi's view of the uncertain world, but replaces its statistical techniques to tackle robustness using metamodels by Kriging. Moreover, to deal with this uncertainty, different approaches have been proposed in robust simulation optimization. Dellino et al. [58, 59] combined Taguchi's world view with regression metamodels in uncertain environment by fitting two Kriging metamodels, one for the mean and one for the variance of the response. To formulate the robust optimization problem, they consider minimizing the mean, while satisfying a constraint on the standard deviation (or vice versa). Dellino et al. [56] Also developed a 'robust' methodology for uncertain environments which uses Taguchi's view of the uncertain world, but replaces his statistical techniques by Response Surface Methodology (RSM) and illustrated the resulting methodology through inventory problems.

Robust optimization (RO) is one of the widely-used approaches to deal rigorously with uncertainty in power systems [60]. Nevertheless, when it comes to HRES planning, only a handful of robust models have been investigated in the literature. Dragičević et al. [61] implemented a single-stage RO approach with budget uncertainty sets to design a HRES that serves an autonomous telecommunication facility. A major enhancement achieved through adaptive, two-stage RO models such as that proposed by Billionnet et al. [7] for designing and operating a stand-alone wind-PV-battery-diesel energy system. In their study, budget uncertainty sets were considered for the uncertainty of demand and renewable generators' supply that bound the demand/supply cumulative deviation throughout the yearly operating cycle.

One of the main drawbacks of robust optimization methods is that the occurrence probabilities of the uncertain parameters are not considered, and a solution is found

based on the feasibility for all the values in the uncertainty set so that the final solution would be over-conservative. A remedy for this concern, which has received attention recently, is a framework referred to as DRO [62]. In DRO, the expected value of a probabilistic cost function is optimized, where the expectation is taken with respect to the worst-case probability distribution from a distributional ambiguity set that is constructed based on historical data or information about the "true" distribution. DRO provides a unifying framework for SP and RO while avoiding some of their shortfalls, i.e. the pessimistic nature of RO as it uses the available data more effectively. More related to the HRES planning problem, Alismail et al. [63] proposed a two-stage DRO model for the allocation of wind farms in a multi-area power system under uncertain wind power and generator forced outages, and used moment-based distributional ambiguity sets.

In practice, probability distributions of parameters are not known, and only historical data are available. This means that the distributions of the uncertain parameters are uncertain themselves. One way to define the distributionally ambiguity set that contains the potential probability distributions of the uncertain parameters is to implement the concept of phi-divergence [64]. Phi-divergence is a function, $I_\phi(\mathrm{p}, \mathrm{q})$, that measures the difference between two probability distributions p and q, which p is the true unknown distribution probability and q is the nominal estimate of p. There are several advantages to use phi-divergences. First, many common phi-divergences are used in statistics, for instance, to conduct goodness-of-fit tests. Therefore, they provide natural ways to deal with data and distributions. Another attractive feature of phi-divergences is that they preserve convexity, resulting in computationally tractable models. Using phi-divergences can also be more data-driven–many since phi-divergences use more distributional information than just the first and second moments [65]. Moghaddam and Mahlooji [66] implemented a phi-divergence ambiguity set and proposed two approaches, a minimax and a chance constraint method, to formulate the robust counterpart problem for the objective function estimated by Kriging.

Going through the literature, phi-divergence ambiguity sets have been used in areas such as production planning [66, 67], lot-sizing [68], finance [69, 64] and inventory control [66]. However, there has been no study so far to investigate the use of DRO

with phi-divergence-based ambiguity sets in HRES planning. The DRO approach used in this thesis specifically target the issue of the uncertain occurrence probabilities of the supply scenarios, which can be attributed to the use of limited sample data to construct these scenarios. Since there has been no study so far to investigate the combination of metamodel approaches with DRO to tackle the lack of explicit objective function and the uncertainty in the probability of supply power scenarios, the current research will be the first to apply this concept in order to avoid the over conservatism issue of RO by using sample of historical data to extract information about the probability distribution of the uncertain parameters.

Chapter 3

Problem description and modelling

In this study, due to the promising and complementary nature of wind and solar, a HRES comprises wind turbines and PV panels with energy storage and a diesel generator to fill in the gap between supply and demand power, is considered. Due to high costs of connection to the long-distance transmission or distribution grid, the proposed system operates in a standalone mode to meet the energy needs in rural remote areas. Also, the stochastic nature of input data, solar and wind, leads to fluctuations in power production and their patterns can be clustered into finite number of scenarios to make handling the supply data easier. In the following, the presumed operational rules for the HRES and scenario generation using clustering approach are presented.

3.1 Operational Rules

Every HRES requires a set of rules to be operated. These rules specify, for example, which energy source is to be utilized when there is a mismatch between the supply of renewable sources and the demand. The HRES under consideration is simulated based on certain operational rules that are presumed to mimic those implemented in reality. However, it is important to note that the mere purpose of using these rules is to enable the estimation of the TAC of the system, and that the proposed robust SO approaches can be used with any set of operational rules, and are not restricted to the specific ones employed here. The set of operational strategies implemented in this thesis are the actual operating rules used in previous studies [34, 30, 70]. The output obtained from one time interval are used as inputs for the next interval and the model can be solved for each time step independently. Supply and demand data time interval for the simulation is considered one hour, which is an acceptable assumption in sizing and optimization of HRES and would reduce the solution time significantly [33, 30, 71]. The priority of the system resources utilization is depicted

Nomenclature

Indices	
$t \in T$	Time period
$s \in S$	Scenario
Parameters	
d_t	Demand Power at time period t (kW)
$P_{t,s}^{PV}$	PV panel power at time period t for scenario s (kW)
$P_{t,s}^{WT}$	Wind turbine Power at time period t for scenario s(kW)
q_s	Nominal probability of scenario s
SC_{bat}	Nominal storage capacity of a battery (kWh)
MR_{bat}	Maximum charge/discharge rate of battery (kW)
$C_{DG,1}$	Initial cost of Diesel Generator ($/kW)
$C_{DG,2}$	Operational cost of Diesel Generator ($/kWh)
C_{PV}	Unit cost of a PV panel ($/Unit)
C_{WT}	Unit cost of a wind turbine ($/Unit)
C_{bat}	Cost of a battery ($/Unit)
L_{bat}	Number of full charging cycle of a battery
η_{bat}	Battery discharging efficiency
Variables	
$Dch_{t,s}$	Discharging power of battery at time period t for scenario s (kW)
$Ch_{t,s}$	Charging power of battery at time period t for scenario s (kW)
$P_{t,s}^{DG}$	Diesel generator power at time period t for scenario s (kW)
$SoC_{t,s}$	Battery state of charge at the beginning of time period t for scenario s (kWh)
$UD_{t,s}$	Unmet demand at time period t for scenario s (kW)
Design Variables	
N_{PV}	Number of PV panels
N_{WT}	Number of wind turbines
N_{bat}	Number of batteries
Cap_{DG}	Capacity of Diesel Generator (kW)

in Figure 3.1:

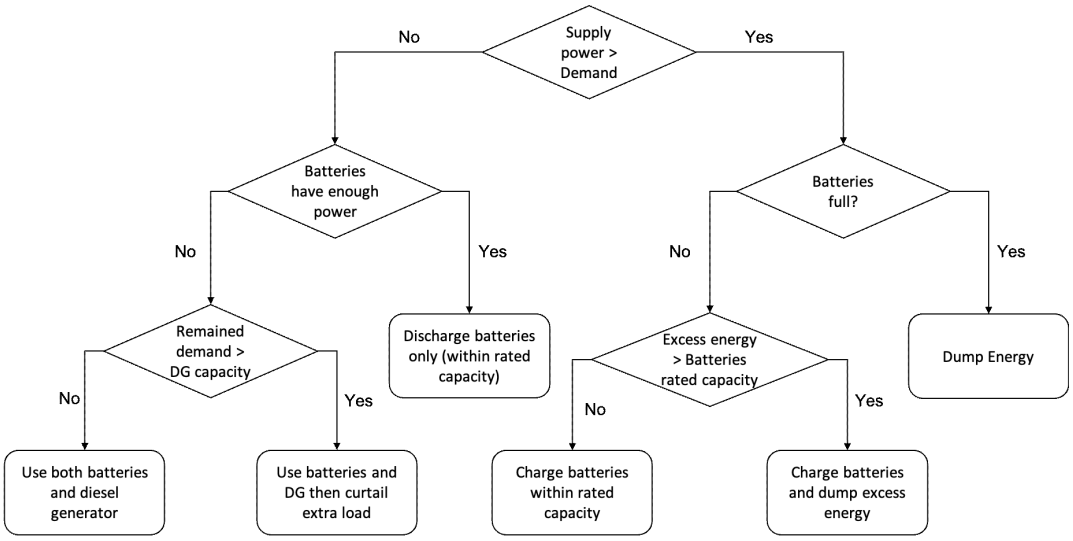

Figure 3.1: Utilization priority of system resources

i In any time interval, if the power demand exceeds the power supplied by the PV panels and wind turbines, the power deficit is compensated, if possible, by the batteries within their rated capacity (maximum charge/discharge rate of each battery), and the remaining load (if any) is met using the diesel generator power. If the remaining demand is more than the diesel generator capacity, the extra loads are curtailed. To discourage load curtailment and ensure high reliability, the amount of curtailed power is multiplied by a penalty factor and added to the total cost. On the other hand, if the power supplied by the PV panels and the wind turbines is greater than the demand, the excess energy is used to charge the batteries if they are not full and within their charging limits, and any remaining energy is dumped.

ii Batteries can be charged only when there is surplus power generated by PV panels and wind turbines and are never charged using the diesel generator. Also they cannot be charged and discharged at the same time.

iii Diesel generator can supply power only when the power discharged by the batteries is not sufficient to meet the remaining demand.

iv Curtailment of loads is not allowed when the power generated by power resources is enough to satisfy them.

v The simulated system cannot dump the energy if any load demand is still not satisfied.

According to the first operational rule, constraints (3.1.1) link the design variables to the operational variables. The charging and discharging rate must not exceed the capacity of the batteries, and state of charge must also be within the energy storage capacity of the batteries. Maximum depth of discharge (DoD) of batteries is considered 100%. The power supplied by the diesel generator must not violate its rated capacity.

$$\begin{aligned} 0 \leq Dch_t &\leq MR_{bat} \cdot N_{bat} && \forall t \in T \\ 0 \leq Ch_t &\leq MR_{bat} \cdot N_{bat} && \forall t \in T \\ 0 \leq SoC_t &\leq SC_{bat} \cdot N_{bat} && \forall t \in T \\ 0 \leq P_{(DG)t} &\leq Cap_{DG} && \forall t \in T. \end{aligned} \tag{3.1.1}$$

Moreover, based on the energy conservation law, the amount of energy stored in a battery is dependent on the amount of energy in the preceding period, and the charging/discharging during the current period. Discharge efficiency of the batteries (η_{bat}) and Δ_t are assumed ideal (i.e., 100%) and one-hour interval, respectively. With that, we use the following energy conservation constraint:

$$SoC_t = SoC_{t-1} + \Delta_t \cdot Ch_t - \Delta_t \cdot \frac{Dch_t}{\eta_{bat}} \qquad \forall t \in T. \tag{3.1.2}$$

The first objective is to minimize the total annual cost (Y^{TAC}). Based on Equation (3.1.3), the first two terms represent the cost of PV panel and wind turbine installation, the third term calculates the batteries cost, assuming they can function for a specific number of full charging cycles before replacement. The last two terms denote two types of costs for the diesel generator: initial and operational. The initial cost of a diesel generator is mainly dependent on its capacity and the operational cost has a linear relationship with the power output of the diesel generator. The amortization parameter $A = \frac{ir}{1-(1+ir)^{-n}}$, where ir and n are, respectively, the interest rate and the

HRES lifetime, is multiplied by capital costs terms to calculate the annualized cost for the diesel and renewable energy sources.

$$Y^{TAC} = A \cdot (C_{PV} \cdot N_{PV}) + A \cdot (C_{WT} \cdot N_{WT}) + \frac{(1+ir) \cdot C_{bat}}{SC_{bat} \cdot L_{bat}} \sum_{t=1}^{T} Ch_t + A \cdot (C_{DG,1} \cdot Cap_{DG}) + \sum_{t=1}^{T} C_{DG,2} P_{(DG)t} + C_{penalty}. \tag{3.1.3}$$

As mentioned earlier, if the demand could not be met using the available resources, the remaining load is curtailed. To combine the two objectives into a single-objective problem, the amount of unmet demand (UD) in every time interval is multiplied by a penalty value (α) and added to the total cost as: $C_{penalty} = \sum_{t=1}^{T} \mathrm{UD}_t \cdot \alpha$. All together, Equation (3.1.4) links the demand and supply quantities, as follows:

$$d_t = N_{PV} \cdot P_t^{PV} + N_{WT} \cdot P_t^{WT} - Ch_t + Dch_t + P_t^{DG} + UD_t \qquad \forall t \in T. \tag{3.1.4}$$

The second objective is to maximize the system reliability. One of the most widely-used reliability indices is the loss of load probability (LLP) which measures the inability of HRES to meet the system load [9]. LLP is used as the reliability objective to be minimized in [15, 16, 17, 18, 19]. Having the amount of total and unmet demand in hand, the value of LLP is calculated at the end of the simulation using the following equation:

$$LLP = \frac{\sum_{t=1}^{T} UD_t}{\sum_{t=1}^{T} d_t}. \tag{3.1.5}$$

In the following, a Pseudocode for the system simulation is included to explain

the input/output relation and operational rules in a clearer way.

Read: P_t^{PV}, P_t^{WT}, d_t;
Input : $N_{PV}, N_{WT}, N_{bat}, Cap_{DG}$
Output: Y^{TAC}, LLP
Calculate $SP_t = N_{PV} \cdot P_t^{PV} + N_{WT} \cdot P_t^{WT}$;
for $t = 1 : T$ **do**
    if $SP_t \leq d_t$ **then**
        $Dch_t = \min(d_t - SP_t,\ MR_{bat} \cdot N_{bat},\ Soc_t)$;
        $SoC_t = SoC_{t-1} - Dch_t$;
        $P_t^{DG} = \min(d_t - SP_t - Dch_t,\ Cap_D G)$;
        $UD_t = d_t - SP_t - Dch_t - P_t^{DG}$;
    else
        $Ch_t = \min(SP_t - d_t,\ MR_{bat} \cdot N_{bat},\ SC_{bat} \cdot N_{bat} - SoC_t)$;
        $SoC_t = SoC_{t-1} + Ch_t$;
    end
end
Calculate Y^{TAC} according to Equation (3.1.3);
Calculate LLP according to Equation (3.1.5);

Algorithm 1: System Simulation

3.2 Stochastic supply model

Power supplied by the PV modules and the wind turbines is intermittent and stochastic. The power generated by a PV panel at any moment is highly variable and difficult to predict accurately due to many factors, including: solar irradiance, incidence angle, cleanness of the PV module surface, shading, and other technical characteristics of the PV module. Also, the highly variable and unpredictable wind speed plays a crucial role in determining the power output of the wind turbine generators, leading to very random patterns of power output. In an ideal condition, every day in a year can be considered as a scenario regardless of high computational time and cost. However, dealing with 365 scenarios results in high computational time and complexity. Instead clustering techniques can be used to extract a small number of scenarios from the data that can be handled effectively. Upon extracting the scenarios, each represents a possible patterns of power supply, and after calculating the probability of each scenario, they can be incorporate in a stochastic optimization model.

One way to define the supply scenarios and determine their probabilities is through k-means clustering. A k-means classification algorithm iteratively tries to partition the dataset into k pre-defined distinct non-overlapping subgroups, and in this study, S scenarios. It is based on the minimization of an objective function defined as [72]:

$$\min \sum_{s=1}^{S} \sum_{n=1}^{N} \mu_{ns} \left\| x_n - v_s \right\|_2, \tag{3.2.1}$$

where x_n is the actual power output in day n and v_s is the center of scenario s. Also μ_{ns} is the assignment variable which equals 1 if the daily profile n is assigned to cluster s and 0 otherwise. Both x_n and v_s are vectors consisting of 24 elements (24 hours per day). This optimization problem can be solved using a heuristic iterative algorithm explained as follows:

1. Specify the number of scenarios and initialize the centroids by randomly selecting S clusters of data points for the centroids without replacement.

2. Calculate the distance (d_{ns}) between each point in a daily profile (x_n) and its

corresponding point of cluster centroid (v_s) as $d_{ns} = \|x_n - v_s\|_1$ and allocate it to the nearest center.

3. Update the centroids using the following transformation (j is the iteration and $[S] = 1, ..., S$):

$$v_s^j = \frac{\sum_{n=1}^{N} \mu_{ns} \cdot x_n}{\sum_{n=1}^{N} \mu_{ns}} \qquad \forall s \in [S] \tag{3.2.2}$$

4. Keep iterating between steps 2 and 3 until there is no change to the centroids and the improvement is less than a certain tolerance ϵ:

$$|\sum_{s=1}^{S}\sum_{n=1}^{N}(d_{ns}^{j+1})^2 - \sum_{s=1}^{S}\sum_{n=1}^{N}(d_{ns}^{j})^2| \leq \epsilon. \tag{3.2.3}$$

5. Calculate the probability of each scenario s as:

$$p_s = \frac{\sum_{n=1}^{N} \mu_{ns}}{N} \qquad \forall s \in [S]. \tag{3.2.4}$$

Since this is a heuristic method, it is very likely to converge to a local optimum. Thus, the clustering algorithm is repeated from different initial cluster centers and the best clustering output is declared optimum. As explained, we begin with a $|S| = 2$ and increase the number of clusters incrementally until they meet the marginal reduction in the variance condition stated in Equation (3.2.3). After determining the optimum number of solar and wind clusters, the total number of supply scenarios is their product.

3.3 Phi-divergence ambiguity set

It should be noted that the accuracy at which the unpredictable nature of PV and WT power supply is captured can be improved by increasing the number of supply scenarios. However, the use of limited data to extract these scenarios poses another challenge related to estimating their probability distribution. Given that the number of data points (daily profiles) in the clustering process is small, even a tiny perturbation in a single data point can lead to a significant change in the probabilities of scenarios (yet probably not much in their centroids). Hence, it is important to

robustify the design model against ambiguity about these probabilities. One way to capture the distributionally ambiguity is to use a phi-divergence ambiguity set. Phi-divergences quantify the difference between a pair of non-negative vectors of the same size, $\mathrm{p} = (p_1, ..., p_S)^T$ and $\mathrm{q} = (q_1, ..., q_S)^T$ where p is the unknown true probability and q is the empirical estimate of p [64]. Formally, a Phi-divergence is defined as:

$$I_\phi(\mathrm{p}, \mathrm{q}) = \sum_{s=1}^{S} q_s \phi(\frac{p_s}{q_s}) \tag{3.3.1}$$

Where $\phi(t)$ is called phi-divergence function and is a convex for $t \geq 0$. An ambiguity set for p defines the family of distribution:

$$P_\phi := \{\mathrm{p} | \mathrm{p} \geq 0, \sum_{s=1}^{S} p_s = 1, I_\phi(\mathrm{p}, \mathrm{q}) \leq \rho\} \tag{3.3.2}$$

Table 3.1, taken from Ben-Tal et al. [64], presents the most common choices of phi-divergence and their conjugate function.

Divergence	$\phi(t), t \geq 0$	$I_\phi(\mathrm{p}, \mathrm{q})$	$\phi^*(s)$
Kullback-Leibler	$t \log t - t + 1$	$\sum p_s \log(\frac{p_s}{q_s})$	$e^s - 1$
Burg Entropy	$-\log t + t - 1$	$\sum q_s \log(\frac{q_s}{p_s})$	$-\log(1-s), s < 1$
χ^2-distance	$\frac{1}{t}(t-1)^2$	$\sum \frac{(p_s - q_s)^2}{p_s}$	$2 - 2\sqrt{1-s}, s < 1$
Variation Distance	$\lvert t - 1 \rvert$	$\sum \lvert p_s - q_s \rvert$	$\begin{cases} -1 & s \leq -1 \\ s & -1 \leq s \leq 1 \end{cases}$
Hellinger Distance	$(\sqrt{t} - 1)^2$	$\sum (\sqrt{p_s} - \sqrt{q_s})^2$	$\frac{s}{1-s}, s < 1$

Table 3.1: Common choice of ϕ-divergence

Most phi-divergences do not satisfy the triangle inequality, and many are not symmetric in the sense that $I_\phi(p, q) \neq I_\phi(q, p)$. However, one exception is the Variation Distance or L^1-distance between the vectors [73], defined as $I_\phi(p, q) = \sum_{s=1}^{S} |p_s - q_s|$. In addition to the linear structure of this function, working with the variation distance has other benefits. It allows $p_s = 0$ for a scenario for which $q_s > 0$, and we may also have $p_s > 0$ for a scenario for which $q_s = 0$ (these situations are called respectively "suppressed" and "popped" scenarios in [73]). Using the variation distance

leads to a computationally tractable optimization model which can be solved by a decomposition algorithm [74]. An ambiguity set based on the Variation Distance phi-divergence is used in the next section.

Chapter 4

Solution Methodology

To solve the problem, the cost and reliability functions for each scenario needs to be evaluated. Since there is neither a closed form expression nor an analytical method to evaluate the TAC and reliability, they have to be estimated through simulation. Statistical approximations, or metamodels, are used to replace the expensive and complex existing real systems, and they yield insight into the functional relationship between inputs and outputs data through simulation [57]. Two different metamodels are fitted on the input/output data and their SO procedures are explained.

4.1 Classical Response Surface Methodology

The Classical RSM was introduced in 1951 by Box and Wilson [75], and was developed for the optimization of real (physical) systems. RSM is one of the most popular methods in simulation optimization and is a step-wise heuristic method that estimates the best inputs combination that minimizes the given objective function. In the final stage it predicts the goal function as a second-order metamodel based on the inputs/output observation. In this study, a robust version of the classical RSM is proposed along with its nominal version. The complete procedure of this method is explained as follows [76]:

1. This approach begins by selecting a starting point. Input selection can be made based on intuition and prior knowledge or a currently used combination in a system.

2. The expected TAC is estimated through calculation of TAC for each scenario ($\hat{Y}_s^{TAC}$), and the following optimization problem is solved to find the worst-case distribution p:

$$Max_{p \in P_\phi} \sum_{s=1}^{S} p_s \hat{Y}_s^{TAC}, \tag{4.1.1}$$

where the variation distance phi-divergence ambiguity set is defined as $P_\phi : \{\mathrm{p}_s \geq 0\,, \sum_{s\in[S]} \mathrm{p}_s = 1,\ \|\mathrm{p}-\mathrm{q}\|_1 \leq \rho\}$. This step is skipped when solving the nominal problem (when there is no uncertainty about the probabilities of scenarios) and the nominal distribution ($\mathrm{q_s}$), obtained from Equation (5), is used instead. An easier approach for finding the worst-case distribution is to simply move $\rho/2$ probability mass from the scenario with the lowest cost to the scenario(s) with the highest cost. Other scenarios' probabilities remain the same.

3. The input/ output behavior of the simulated system is explored in the neighborhood of the starting point. This behavior is approximated through the local first-order polynomial

$$\hat{Y}_s^{TAC} = \beta_{0,s} + \sum_{i=1}^{n} \beta_{i,s} X_{i,s} + e_s \qquad \forall s \in [S], \tag{4.1.2}$$

where e is the white noise assumed normally i.i.d. random variables with a zero mean and a constant variance, $e \sim NIID(0, \sigma^2)$. To estimate the intercept ($\beta_{0,s}$) and slope ($\beta_{i,s}$) coefficients of the polynomial function for any scenario, a Resolution-III design is used. In classical R-III designs, the number of combinations is a multiple of four and in the standardized inputs X_i, '-' means -1 (minimum level) and '+' means +1 (maximum level). The design is "balanced," i.e., each column has n/2 values equal to -1. Moreover, all pairs of columns are orthogonal. Figure 4.1 illustrates the R-III design for three factors.

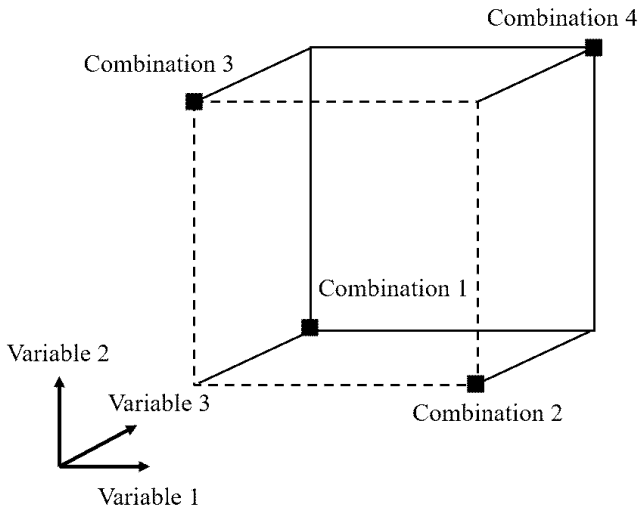

Figure 4.1: A fractional-factorial two-level design for three variables

In this study, four input variables (N_{pv}, N_{wt}, N_{bat}, and Cap_{DG}) are considered, and according to Table 4.1, R-III design for four variables has eight combinations.

Combination	1	2	3	4 = 1.2.3
1	-	-	-	-
2	-	-	+	+
3	-	+	-	+
4	-	+	+	-
5	+	-	-	+
6	+	-	+	-
7	+	+	-	-
8	+	+	+	+

Table 4.1: A fractional factorial design for four factors

After calculating all the eight outputs from different input combinations, the n main effects β_i can be estimated using the Least Squares (LS) method, which gives the best linear unbiased estimator (BLUE) of

$$\hat{\beta} = (X^T X)^{-1} X^T y, \tag{4.1.3}$$

where X denotes the $8 \times (4+1)$ matrix determined by the R-III design, representing the vector with the eight simulation outputs. After fitting a plane

for each scenario, the weighted average linear equation $\hat{Y}^{TAC} = \sum_{s=1}^{S} p_s \hat{Y}_s^{TAC}$ ($\hat{Y}_s^{TAC}$ is a function of X) is calculated using the weights (p) from step 2.

4. A steepest descent method using the local gradient is applied to explore the next input combination. The steepest descent direction is $-\Delta = -[\beta_1, \beta_2, \beta_3, \beta_4]$, where the coefficients are calculated in the previous step. As we move in the steepest descent direction for the step size t, i.e., $X_{new} = X_{old} - \Delta \cdot t$, the new configuration (X_{new}) is calculated. Unfortunately, the steepest descent technique does not quantify the step size along its path. The analysts may therefore try some intuitively selected value for the step size. To tackle this problem, Kleijnen et al. [77] and Kleijnen [78] proposed novel techniques called "adapted" steepest ascent/descent combining mathematical statistics and mathematical programming accounts for the covariances between the components of the estimated local gradient to calculate the step size explicitly. A simpler approached, derived from Bashiri and Samaei [79] and Kleijnen [80], determines the initial step size of X_k based on the process characteristic and other control variables' step sizes are determine by

$$\Delta X_i = \frac{\Delta X_k}{\beta_k} \beta_i \qquad i = 1, \ldots, n. \tag{4.1.4}$$

In this study, $\frac{\Delta X_k}{\beta_k}$ is set equal to $\min[\frac{\Delta X_i}{\beta_i} \quad i = 1, \ldots, n]$ where ΔX_i demonstrates the increment size of the system components which is the smallest allowed quantity to change the component size. For example, the increment for PV panels can be a 10kW unit, for wind turbine can be a 50kW turbine, for batteries can be a 165kW module, and for DG can be a 10kW unit.

5. The new point (X_{new}) is evaluated through simulation. If there is an improvement compared to the current solution, the search continues in the same direction by setting $X_{new} = X_{old} - \Delta \cdot 2t$ as the new trial point. However, if there is no improvement (i.e., the simulation output deteriorates) the trial point of the previous step is considered the optimal solution found until now.

6. However, it is intuitively clear that a local first-order polynomial cannot adequately represent a hilltop (when searching for the maximum and, in this study, the minimum). So in the neighborhood of the optimum, the gradient

of first-order polynomial becomes small and shows a serious lack of fit. When the most recently fitted first-order polynomial turns out to be inadequate, a second-order polynomial is fitted on the subarea. To estimate this metamodel, a combination specified by a Central Composite Design (CCD) is simulated and the following quadratic formula is fitted:

$$\hat{Y}_s^{TAC} = \beta_{0,s} + \sum_{i=1}^{n} \beta_{i,s} X_i + \sum_{i=1}^{n} \sum_{j=1}^{i} \beta_{ij,s} X_i X_j + e_s \qquad \forall s \in [S]. \qquad (4.1.5)$$

A CCD augments a Resolution-V design such that the purely quadratic effects can be estimated. In general, a CCD adds the central point and $2n$ axial points that form a star design. Wherein the coded factors, the central point is (0,. . . ,0), and the "positive" axial point for factor i (with $i = 1, ..., n$) is the point with $X_i = +c$ and all other $n - 1$ factors fixed at the center and the "negative" axial point for factor i is the point with $X_i = -c$ and $X_{i'} = 0$ (See Figure 4.2 for an illustration). Selecting $c = k^{1/2}$ results in a rotatable design;

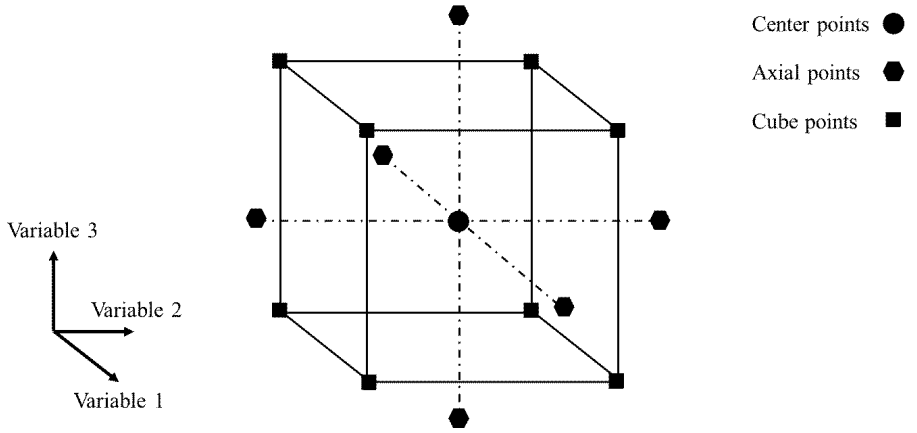

Figure 4.2: Central Composite Design for three variables

i.e., this design gives a constant variance for the predicted output at a fixed distance from the origin (so the contour functions are circles). Note that a CCD does not give an orthogonal X; hence, the estimated parameters of the second-degree polynomial are correlated. Note further that the central point in the cube is replicated to estimate the common variance and to compute the lack-of-fit F-statistic. As mentioned earlier, DOE provides designs with three values per factor for second-order metamodel estimation. However, in

Central Composite Designs (CCDs), there are five values per factor, which means axial points ($c = 4^{1/2}$ and$-c = -4^{1/2}$) are also considered for a rotatable design. The second-order polynomial in Equation (4.1.5) is nonlinear in X but linear in β. Consequently, such a metamodel remains a linear regression model and, again, Least Squares (LS) method would give the best linear unbiased estimator (BLUE) of β as in Equation (4.1.3). Having four design variables, 15 coefficients of β are estimated for quadratic polynomial. Figure 4.2 illustrates a CCD for three parameters. The weighted quadratic equation is calculated as $\hat{Y}^{TAC} = \sum_{s=1}^{S} \mathrm{p_s} \hat{Y}_s^{TAC}$.

7. Using the first order optimality condition, $\hat{Y}^{TAC}(X)$ is differentiated to obtain the gradient, which is then equated to zero. By solving four simultaneous equations, the optimal solution and decision variables are obtained.

For a better comprehension of the proposed classical RSM algorithm, a pseudocode description (Algorithm 2) and a flowchart (Figure 4.3) are presented below.

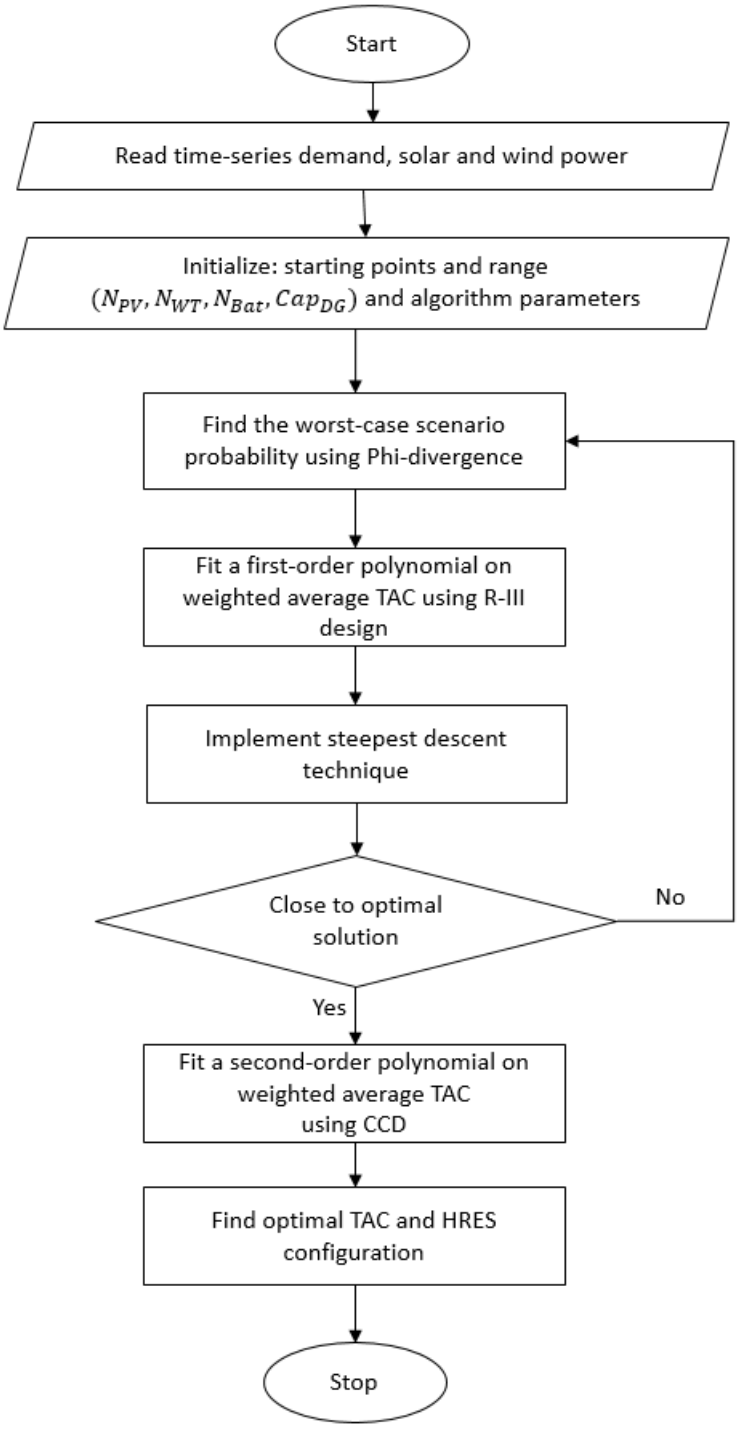

Figure 4.3: A flowchart of the Classical RSM

read: Solar, wind, and demand power data for all scenarios;
input : q_s
output: $\hat{Y}^{TAC}, X_i$
Initialize starting points X;
Initialize gradient;
while *gradient* $\leq \varepsilon$ **do**
    foreach *scenario* $s \in [1, \ldots, S]$ **do** Calculate `TotalAnnualCost(`*starting points*`)`;
    Solve (4.1.1) to get the worst-case distribution;
    Generate a set of sample points with R-III design;
    for *each scenario* $s \in [1, \ldots, S]$ **do**
        Calculate `TotalAnnualCost` function evaluation;
        Fit a first-order polynomial;
    end
    Calculate the weighted average first-order equation using p;
    Apply Steepest Descent to get a new combination X_i^*;
    Update gradient;
    Update X_i;
    Replace initial points with the best combination found so far;
end
Generate a set of sample points with Central Composite Design;
for *each scenario* $s \in [1, \ldots, S]$ **do**
    Calculate `TotalAnnualCost` function evaluation;
    Fit a second-order polynomial;
end
Calculate the weighted average second-order equation;
Solve the second-order polynomial to get the optimal HRES combination X_i and $\hat{Y}^{TAC}$

Algorithm 2: Classical RSM

4.2 Global Response Surface Technique (GRST)

Several approximation approaches have been introduced in the past to simulate real-world examples. One of the most popular methods for using complex simulations is the broad category of optimization algorithms based on cheap global approximation models - often called surrogate models – of simulation. These models investigate the unknown relationship between a set of variables and the system output and use this training data to build a surrogate model, which is cheap to evaluate. A detailed classification of optimization methods based on global approximation models is provided by Jones [81]. GRST is an exploratory global approximation model, that unlike the classical RSM described in the previous section, fits a convex second-order polynomial on the entire search space from the beginning. The process is explained in two phases:

1. First, an initial set of sample points is generated using some Design of Experiments (DoE) technique. At this stage, the location of the points is only required to satisfy some space-filling criterion. A wide variety of DoE methods are available to the designer wishing to select the initial sample points. The Latin Hypercube Sampling (LHS) is amongst the most widely used designs. It ensures that the set of random numbers represent the real variability and new sample points are generated by taking into account the previously generated sample points. This sampling method is used for Monte Carlo integration. In performing Monte Carlo simulation (MCS), it is assumed that each variable has a uniform distribution with corresponding lower (X_i^l) and upper (X_i^u) limits and accordingly, random sample points are generated as:

$$X_i = X_i^l + \alpha X_i^u \qquad i = 1, ..., n, \tag{4.2.1}$$

where $\alpha \in [0, 1]$ is a random number. It worth mentioning that the search space is the same for all scenarios. Upon evaluating the cost function for the selected random points, a convex quadratic surrogate model is fit over the feasible design area for every scenario, $\hat{Y}_s^{TAC}(X)$, using the least square method as

$$\begin{aligned} &\min \left\| Y_s^{TAC}(X) - \hat{Y}_s^{TAC}(X) \right\|_2 \\ &\text{s.t.} \quad \mathrm{H}_s(\hat{Y}^{TAC}) \ \text{ is positive semi-definite}(n) \quad \forall s \in [S], \end{aligned} \tag{4.2.2}$$

which is fully quadratic with $(n+1)(n+2)/2$ coefficients and n is the number of design variables. To have a convex function, the Hessian matrix of the quadratic function ($\mathrm{H}_s(\hat{Y}^{TAC})$) must be positive semi-definite. In this approach, $\hat{Y}^{TAC}$ is a convex function of 4 variables for a total of 15 unknown coefficients as follows:

$$\begin{aligned}\hat{Y}^{TAC}(X) =&\beta_0 + \beta_1 X_1 + \beta_2 X_2 + \beta_3 X_3 + \beta_4 X_4 + \beta_5 X_1 X_2 + \beta_6 X_1 X_3 \\ &+ \beta_7 X_1 X_4 + \beta_8 X_2 X_3 + \beta_9 X_2 X_4 + \beta_{10} X_3 X_4 + \beta_{11} X_1^2 \\ &+ \beta_{12} X_2^2 + \beta_{13} X_3^2 + \beta_{14} X_4^2.\end{aligned} \tag{4.2.3}$$

Positive semi-definite attribute of the quadratic function Hessian matrix is assured as:

$$\mathrm{H}_s(\hat{Y}^{TAC}) = \begin{bmatrix} 2\beta_{11} & \beta_5 & \beta_6 & \beta_7 \\ \beta_5 & 2\beta_{12} & \beta_8 & \beta_9 \\ \beta_6 & \beta_8 & 2\beta_{13} & \beta_{10} \\ \beta_7 & \beta_9 & \beta_{10} & 2\beta_{14} \end{bmatrix} \succcurlyeq 0. \tag{4.2.4}$$

In the nominal problem, the objective function is defined as the weighted sum of the S fitted surrogate functions, whose weights are the empirical occurrence probability of supply power (q) as:

$$\min \hat{Y}_{TAC}(X) = \sum_{s=1}^{S} q_s \hat{Y}_s^{TAC}(X) \tag{4.2.5}$$

However, in the robust problem, the probabilities are not known in advance and must be calculated. Using Variation Distance to define the phi-divergence ambiguity set, the robust counterpart for Equation (4.2.5) would be:

$$\begin{aligned} \min_X \max_{\mathrm{p}} & \sum_{s=1}^{S} p_s \hat{Y}_s^{TAC}(X) \\ \text{s.t.} \quad & \sum_{s=1}^{S} p_s = 1 \\ & \sum_{s=1}^{S} |p_s - q_s| \le \rho \\ & p_s \ge 0. \end{aligned} \tag{4.2.6}$$

The new variable γ_s is defined to linearize the absolute value term $|p_s - q_s|$, thus the inner optimization problem becomes

$$\begin{aligned} \min_X \max_{\mathrm{p}} & \sum_{s=1}^{S} p_s \hat{Y}_s^{TAC}(X) \\ \text{s.t.} \quad & \sum_{s=1}^{S} p_s = 1 && \rightarrow \quad (\eta) \\ & \sum_{s=1}^{S} \gamma_s \leq \rho && \rightarrow \quad (\delta) \\ & -\gamma_s + p_s \leq q_s && \rightarrow \quad (\pi_s) \\ & -\gamma_s - p_s \leq -q_s && \rightarrow \quad (\alpha_s) \\ & p_s, \gamma_s \geq 0. \end{aligned} \tag{4.2.7}$$

Based on LP duality, the robust optimization problem is tractably reformulated as:

$$\begin{aligned} \min \ & \eta + \rho\delta + \sum_{s=1}^{S} (q_s(\pi_s - \alpha_s)) \\ \text{s.t.} \quad & \hat{Y}_s^{TAC}(X) - \eta - \pi_s + \alpha_s \leq 0 && \forall s \in [S] \\ & -\delta + \pi_s + \alpha_s \leq 0 && \forall s \in [S] \\ & x, \delta, \pi_s, \alpha_s \geq 0. \end{aligned} \tag{4.2.8}$$

2. The second phase entails restricting the search space around the optimum configuration found in the previous iteration. This occurs by reducing the search space and defining a new range for design variables based on the optimum solution found so far. This procedure is then repeated until the termination criterion is satisfied. A pseudocode of the GRST is provided in Algorithm 3. Examples for termination criteria are either negligible difference between upper and lower bound of all variables, which can be written as

$$|X_i^u - X_i^l| \leq \varepsilon \qquad i = 1, ..., n, \tag{4.2.9}$$

or when the global optimum found converges *i.e.,* the difference between optimum solutions from the previous iteration is insignificant. When the termination criterion is met, the optimal $\hat{Y}^{TAC}$ and HRES combinations X_i are reported as the optimization results. A flowchart of the GRST is presented in Figure 4.4.

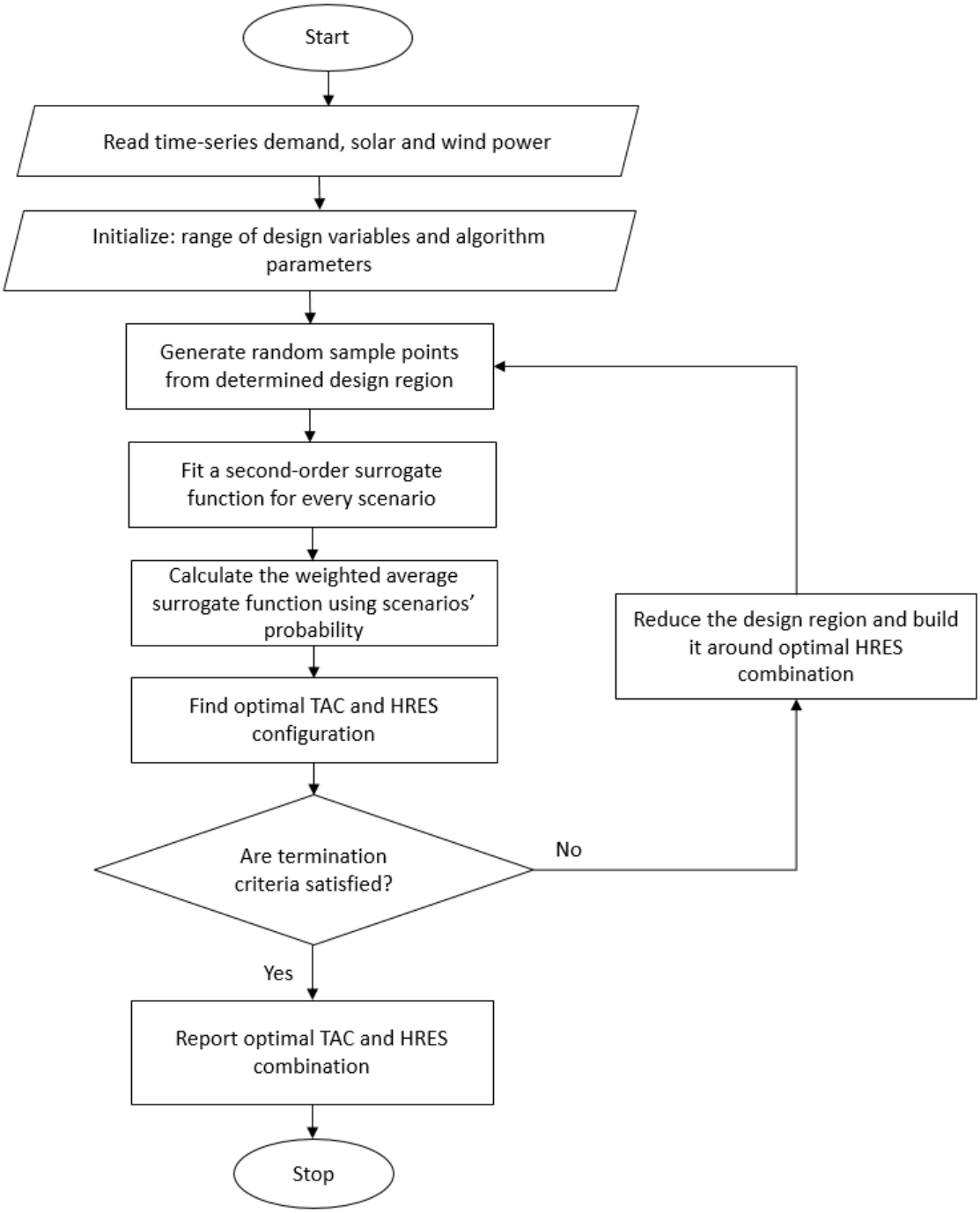

Figure 4.4: A flowchart of GRST

Read: Solar, wind, and demand power data for all scenarios;
Input : Nominal scenario's probability q
Output: $\hat{Y}^{TAC}, X_i$
Initialize range of design variables as
$X := X \in R_+^n : X_i \in [X_i^l, X_i^u],\ \forall i \in [1, ..., n]$;
Set $X_i^t = \frac{X_i^l + X_i^u}{2}$ and $X_i^r = \frac{X_i^u - X_i^l}{2}$;
Set $X_i^* = X_i^u$ **while** $\|X_i^* - X_i^t\| \mid \geq \varepsilon$ **do**
    $X_i^* \leftarrow X_i^t$
    Generate a set of sample points using LHS from the design space;
    for *each scenario* $s \in [1, \ldots, S]$ **do**
        Calculate `TotalAnnualCost` function of evaluation;
        Fit a second-order surrogate function;
    end
    Solve the nominal problem as in (4.2.5) and robust problem as in (4.2.8) ;
    $X_i^r \leftarrow \frac{X_i^r}{2}$;
    Update X_i^l and X_i^u as $X_i^l = max(0, X_i^t - X_i^r)$ and $X_i^u = X_i^t + X_i^r$;
end
Report the optimal HRES combination X_i and $\hat{Y}^{TAC}$

Algorithm 3: Global Response Surface Technique

Chapter 5

Case study and results

The proposed approaches are tested on a hypothetical case study in northwestern Ontario, Canada, which is the province's most sparsely-populated region.

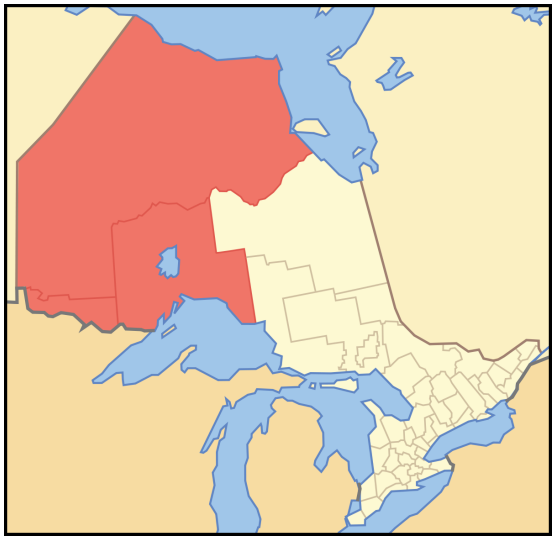

Figure 5.1: Northwestern Ontario

Solar, wind and demand power data are extracted from the Independent Electricity System Operator (IESO) data directory [82] which works closely with Ontario's power system. Demand data is drawn from zonal demand reports which contain hourly zonal demands, derived from operational meters, for the 10 zones in the province, and one-year data related to Northwest Ontario demand is separated and exploited from January 1, 2019 to December 31, 2019. Supply power output of solar and wind is extracted, cleaned, organized and used from Generator Output and Capability Reports [83] which provides hourly output levels, grouped by fuel type, with a maximum output capability of 50 kW and 1 kW for wind turbines and PV panels, respectively for the same year. Reported power is the facility's one-hour outputs based on demand data and total, peak and average load demand are 4,428,870kWh, 734 kW and 505 kW, respectively. The size of the community this system serves is

around 50,000 people. NaS battery modules, a high-temperature rechargeable battery that uses sodium for the negative and sulfur for the positive electrode [84] are used as storage system. High power density, long battery lifetime (usually over 10 years), high efficiency of charge/discharge (up to 90%) and fabricated from inexpensive materials have primarily made NaS batteries suitable for stationary energy storage applications. The last complementary element is a diesel generator to fill the gap between supply and demand power are also considered as resources in this study. Other parameters used to calculate the TAC are depicted in Table 5.1. The costs of PV panels, wind turbines and the diesel generator are obtained from Unplugged Power Systems [85], Atlantic Canada's leader in alternative energy and characteristics related to storage system is extracted from NGK Insulator, LTD [84].

Parameter	Unit	Value
C_{PV}	\$/kW	2000
C_{WT}	\$/kW	2200
C_{bat}	\$/kW	1000
$C_{DG,1}$	\$/kW	350
$C_{DG,2}$	\$/kW	0.182
SC_{bat}	kWh	200
MR_{bat}	kW	33
L_{bat}	Full cycle	4500
n (Useful HRES lifetime)	years	20

Table 5.1: Model parameters

5.1 Generation of Supply Scenarios

Since wind and solar resources are not constantly available and predictable, they are referred to as intermittent energy resources. Under ideal conditions, each daily profile can be considered a separated scenario to provide a comprehensive solution appropriate for all circumstances. However, due to the high computational complexity of large input data, and the time and cost limitations, clustering method is used to decompose the data variability into a small number of scenarios. As the number of clusters increases, the variance between the centroids and points decreases, yet, the computational burden increases too. Therefore, it is important to select

an appropriate number of clusters to minimize within-cluster variance while being computationally tractable. To do this, the k-means clustering process starts with a small number of clusters and increases it incrementally until a certain threshold is met, namely the reduction in the variance is 10% or lower relative to the previous number of clusters. According to Figures 5.2 (a) and (b), the clustering algorithm is applied on both the PV panels and the wind turbine power output data using different number of clusters ranging between 2 and 6. 1000 replications of the clustering procedure are run in order to avoid being trapped in local optima. The optimum number of clusters found are four and three for PV panels and wind turbines power, respectively.

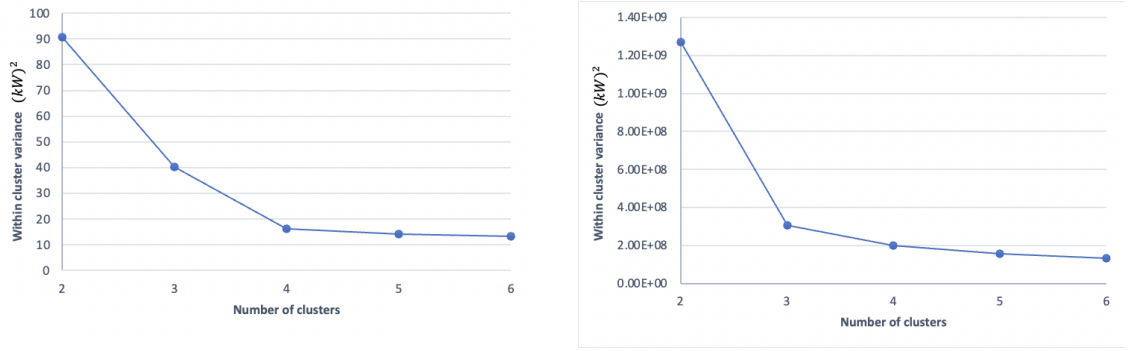

(a) PV panels (b) Wind turbine

Figure 5.2: Variance of within-cluster sums of point-to-centroid distances

Due to the negligible influence of wind speed on solar radiation [86], PV and wind scenarios are assumed independent and $Pr(\text{scenario}_{ij}) = Pr(\text{PV scenario}_i) \cdot Pr(\text{wind scenario}_j)$. Therefore, the PV data is clustered into four groups and the wind data is clustered into three groups, resulting in a total of $4 \times 3 = 12$ scenarios. Figure 5.4 illustrates the centroids of the extracted clusters for both the PV panels and the wind turbines power.

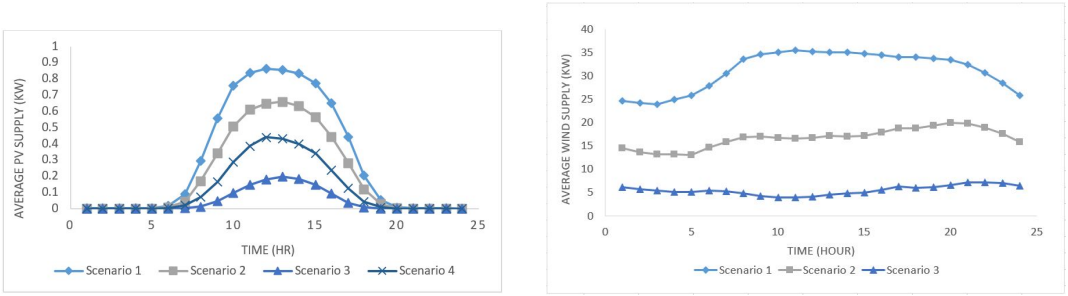

(a) PV panels (b) Wind turbine

Figure 5.3: 24-element supply power centroid extracted from the time-series data

In order to generate annual power supply data, different members (days) are selected randomly from their assigned cluster with replacement, and placed in succession 365 times. This makes a total of $365 \times 24 = 8760$ power output data points with one-hour intervals. It is worth mentioning that members (days) cannot be selected randomly from different clusters in scenario creation since we do not know which probability distribution to use in advance. Figure 5.4 illustrates the yearly power supply profiles corresponding to the extracted scenarios, which are used in this case study.

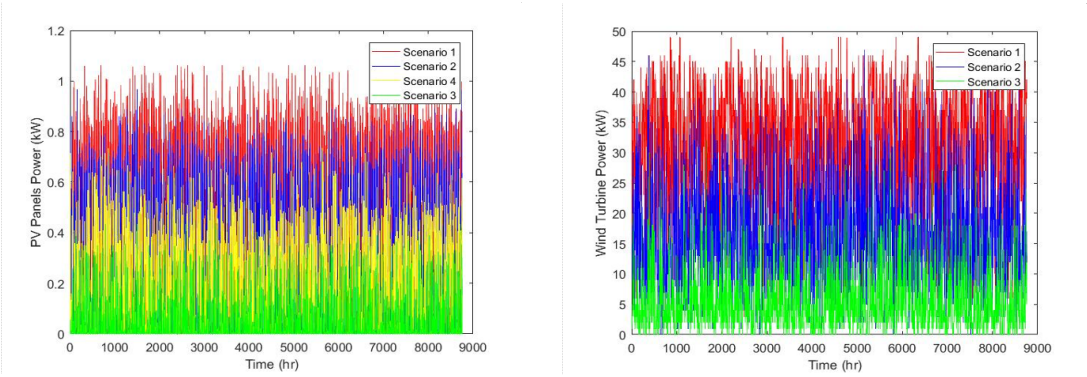

(a) PV Panels (b) Wind turbine

Figure 5.4: Generated annual supply power output

The probability of each supply power cluster is calculated in Table 5.2, which makes the probability of scenarios a product of the related solar and wind clusters. As an example, the probability of Scenario 2, which uses the supply power information of PV panels' first cluster and wind turbine's second cluster is the product of both

probabilities: $0.293 \times 0.353 = 0.103$. If the solar power is categorized into four groups of high, medium, low and very low due to solar irradiance, 107 days of the year power generated from PV panels are at their highest level, 85 days are at medium, 82 days are at low and 91 days are at very low level in power generation. The same conclusion is derived for wind clusters. The extracted supply power scenarios are used as inputs in both approaches for metamodel fitting and optimization process in the next two subsections.

	No. PV members (out of 365)	Probability PV	No. WT members (out of 365)	Probability WT
Cluster 1	107	0.293	64	0.175
Cluster 2	85	0.233	129	0.353
Cluster 3	82	0.225	172	0.471
Cluster 4	91	0.249	-	-

Table 5.2: Number of members and probabilities of clusters

5.2 Classical RSM Results

The simulation and optimization algorithms are coded using Matlab and run on an Apple machine having a M1 chip with 8-core CPU, 8-core GPU and 16-core Neural Engine. Applying classical RSM as the first method, the optimization problem (4.1.1) is solved with Gurobi solver which uses the simplex and interior point methods for solving linear programming problems [87]. The final quadratic function is solved using the first order optimality condition. The design factors and levels considered for Resolution III (R-III) and Central Composite Design (CCD) are demonstrated in Tables 5.3 and 5.4. As an example for R-III design, if the starting point is (N_{PV} =200, N_{WT} =40, N_{bat} =650, Cap_{DG} =600), minimum and maximum level of search space would be (190, 38, 520, 585) and (210, 42, 715, 630), respectively. Similar calculation is made for CCD. Also, 16 cube, 12 central and 8 axial points are the total number of combinations used in CCD for classical RSM.

Design variables	Level	
	Minimum	Maximum
N_{PV}	-5%	+5%
N_{WT}	-5%	+5%
N_{bat}	-10%	+10%
Cap_{DG}	-5%	+5%

Table 5.3: Factors and Levels for R-III

Design variables	Level				
	-2	-1	0	+1	+2
N_{PV}	-10%	-5%	0	+5%	+10%
N_{WT}	-10%	-5%	0	+5%	+10%
N_{bat}	-20%	-10%	0	+10%	+20%
Cap_{DG}	-10%	-5%	0	+5%	+10%

Table 5.4: Factors and Levels for CCD

The results of solving and optimizing each scenario separately with classical RSM

is summarized in the next three tables for three different penalty values. To combine the two objectives into a single-objective problem, these values were selected to demonstrate the trade-off between minimizing TAC and maximizing reliability, otherwise higher values always lead to a 100% reliability. The optimal configuration, best TAC, computational time required for every scenario, number of iteration in steepest descent approach, level of reliability and step size used for every scenario in steepest descent approach are reported in the columns of Table 5.5 for a penalty factor $40 per kWh.

Approach	Scenario # (PV#.WT#)	N_{PV}	N_{WT}	N_{bat}	Cap_{DG} (kW)	TAC	Time (s)	No. iteration	Reliability	Starting point	Step size
	1 (1.1)	232	18	298	222	$159,820	10.18	9	100%	[250,25,380,300]	1.4328e-03
	2 (1.2)	272	33	402	183	$270,923	10.02	9	100%	[300,40,500,250]	1.4337e-03
	3 (1.3)	462	52	904	698	$564,582	13.22	6	100%	[400,75,800,600]	0.07282
	4 (2.1)	162	21	385	367	$179,243	9.69	8	100%	[200,25,420,400]	1.4332e-03
	5 (2.2)	236	35	337	373	$289,021	10.73	13	100%	[300,45,400,400]	1.4317e-03
Classical	6 (2.3)	537	60	708	737	$600,874	9.65	7	100%	[550,80,700,600]	5.0448e-03
RSM	7 (3.1)	242	20	244	353	$180,134	10.50	12	100%	[300,30,300,400]	1.4291e-03
	8 (3.2)	250	38	354	407	$310,120	10.21	10	100%	[300,45,400,450]	1.4332e-03
	9 (3.3)	687	81	1084	694	$707,362	10.08	8	100%	[500,85,700,700]	4.8258e-03
	10 (4.1)	263	19	265	326	$181,212	10.07	8	100%	[300,25,300,350]	1.4332e-03
	11 (4.2)	372	28	594	655	$284,182	10.00	7	100%	[400,35,600,600]	1.8709e-03
	12 (4.3)	611	70	768	396	$638,476	10.83	11	99.22%	[600,80,650,850]	2.3730e-03

Table 5.5: Optimal results for each scenario with $ 40/kWh penalty value

In the classical RSM, a starting point must be selected based on prior knowledge in order to initiate the process. Its selection depends on the intensity of input power data, therefore, it varies for different scenarios. Scenarios with high power generated by renewable energy sources need fewer number of PV panels and wind turbines and accordingly, they start with smaller starting point. The number of iterations, computational time and the step size for each scenario are highly dependent on the starting points. The further the starting point is selected from the optimal configuration, the more time, number of iterations and larger step size (similar to step size of scenario 3 in Table 5.5) are needed to come closer to the final point. The step size in the last column is calculated similar to the fourth step of classical RSM and Equation (4). The number of energy sources during the steepest descent approach is rounded in every iteration rather than once at the end. The optimal

solution reported in the TAC column is without a penalty, i.e. for scenarios with reliability less than 100%, the penalty cost is deducted from TAC and the actual cost is presented. According to this Table 5.5, scenario nine, which uses the third cluster of both PV panels and wind turbine power output, has the highest cost amongst all scenarios, whereas the first scenario, which used the supply data from first cluster of both PV panels and wind turbine power, has the lowest cost.

Approach	Scenario # (PV#.WT#)	N_{PV}	N_{WT}	N_{bat}	Cap_{DG} (kW)	TAC	Time (s)	No. iteration	Reliability
	1 (1.1)	130	13	148	68	$138,577	13.11	14	95%
	2 (1.2)	205	24	344	124	$232,021	15.09	18	95%
	3 (1.3)	376	46	776	432	$561,172	10.20	12	93%
	4 (2.1)	155	14	298	409	$135,294	14.07	15	94%
	5 (2.2)	204	25	405	238	$263,735	17.21	23	93%
Classical	6 (2.3)	300	57	410	383	$585,712	10.39	10	94%
RSM	7 (3.1)	209	13	202	328	$177,075	15.21	19	94%
	8 (3.2)	208	23	287	337	$278,461	18.31	25	93%
	9 (3.3)	230	49	442	527	$691,383	19.43	28	95%
	10 (4.1)	140	15	246	98	$156,023	10.61	12	94%
	11 (4.2)	300	23	347	236	$272,124	11.09	12	95%
	12 (4.3)	209	42	402	378	$664,463	18.23	25	94%

Table 5.6: Optimal results for each scenario with $20/kWh penalty value

Choosing a high penalty cost ($40/kWh) for unmet demand has led to 100% system reliability for almost all the scenarios since a large penalty must be incurred for supply deficiency. Thus, lower values ($20 and $10) of penalty per kWh are also tested and the results are presented in Tables 5.6 and 5.7. The same starting points are used for these two tables. We notice that due to the lower value of penalty cost, fewer number of sources are installed and accordingly, the TAC has reduced while the system reliability has also decreased.

Approach	Scenario # (PV#.WT#)	N_{PV}	N_{WT}	N_{bat}	Cap_{DG} (kW)	TAC	Time (s)	No. iteration	Reliability
Classical RSM	1 (1.1)	106	12	85	25	\$118,899	15.21	16	83%
	2 (1.2)	170	21	220	65	\$213,762	16.26	20	84%
	3 (1.3)	220	40	334	187	\$523132	16.02	19	83%
	4 (2.1)	123	13	386	20	\$129,249	12.74	14	84%
	5 (2.2)	102	22	297	134	\$255,326	18.23	25	85%
	6 (2.3)	232	55	318	135	\$538,153	11.83	12	84%
	7 (3.1)	163	14	107	160	\$169,224	15.67	19	84%
	8 (3.2)	140	21	228	148	\$276,822	19.68	27	86%
	9 (3.3)	208	40	303	283	\$645,428	22.65	32	85%
	10 (4.1)	38	13	136	45	\$148,130	12.25	14	83%
	11 (4.2)	232	21	332	85	\$263,328	12.61	15	84%
	12 (4.3)	141	30	413	256	\$625,923	21.05	30	85%

Table 5.7: Optimal results for each scenario with \$10/kWh penalty value

When considering no ambiguity in the probabilities of scenarios, the best system configuration found using the classical RSM for the nominal problem consists of 404 PV panels, 27 wind turbines, 642 battery modules and a diesel generator with 655 kW capacity, resulting in a TAC of \$472,365 with \$40/kWh penalty cost and 99.99% LLP. As the penalty cost is decreased, the system tendency for allowing supply shortage increases, which leads to a TAC of \$452,041 for \$20/kWh penalty cost and 95.06% LLP and a TAC of \$413,673 for \$10/kWh penalty cost and 84.53% LLP. A summary of the nominal problem results for different penalty values is demonstrated in Table 5.8.

	Penalty cost	N_{PV}	N_{WT}	N_{bat}	Cap_{DG} (kW)	TAC	Iteration	Time (s)	Reliability	Starting point	Step size
Classical RSM	\$40/kWh	404	27	642	655	\$472,364	14	389.32	99.99%	[500,40,750,750]	2.85e-03
	\$20/kWh	322	22	405	350	\$452,041	20	522.03	95.06%	[500,40,750,750]	2.85e-03
	\$10/kWh	243	18	330	245	\$413,673	25	633.29	84.53%	[500,40,750,750]	2.85e-03

Table 5.8: Nominal problem optimal cost and configuration

However, when there is uncertainty, it is important to have the ambiguity set

as small as possible but not too small. Setting $\rho = 0$ obtains the risk-neutral expected value minimization of a stochastic programming problem using the nominal distribution (i.e. the phi-divergence between p and q is zero). At the other extreme, as $\rho \to \infty$, the ambiguity set P_ϕ admits all possible distributions. The worst case among all possible distributions is to move all the probability mass to the scenario with the highest objective function value and set the probabilities of all the other scenarios to zero. This gives the most risk-averse approach and clearly shows the role of ρ as a risk-level parameter [73]. In this study, the highest value considered for ρ is 2, in which case all the probability mass is guaranteed to be moved to the scenario with the highest TAC. The idea is to select an ambiguity set to reflect the perceived risk from the data [73]. Towards this purpose, a sensitivity analysis is performed on different values of ρ to determine the optimal TAC found based on different sizes of the ambiguity set. Figure 5.5 illustrates a sensitivity analysis for three different penalty cost on ρ using the classical RSM approach.

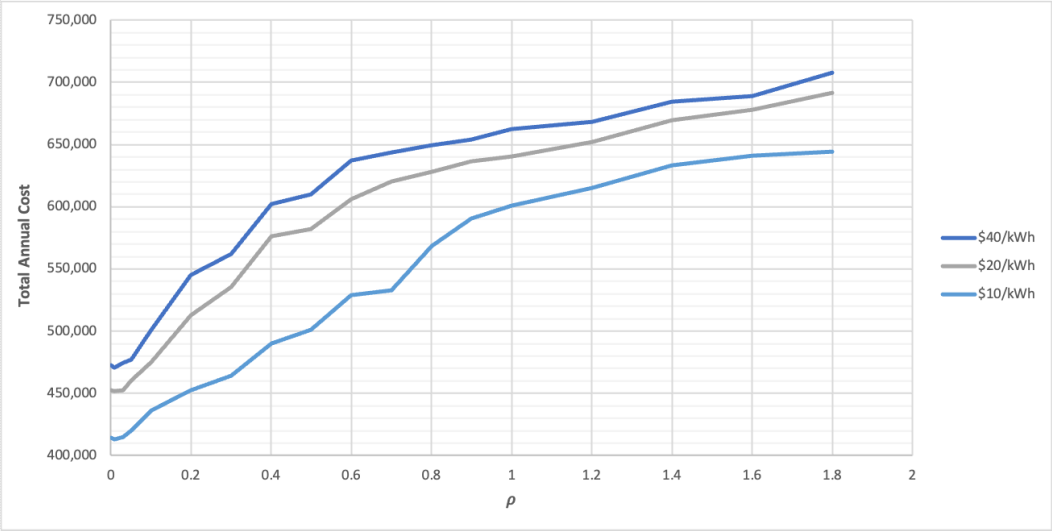

Figure 5.5: Classical RSM: Sensitivity analysis on ρ

As explained earlier, when $\rho = 0$ for a \$40/kWh penalty cost, TAC is \$472,521 which is quite close to the nominal problem (\$472,364), whereas as ρ approaches 2 (\$708,054 for $\rho = 1.8$), the ambiguity set admits all possible distributions and TAC becomes close to that of the worst-case scenario, scenario 9 in Table 5.5, with TAC of \$707,362. The same explanation goes to the problems with \$20/kWh and \$10/kWh penalty factors. In the case with \$20 penalty cost, when $\rho = 0$, TAC is \$452,276

which is close to nominal problem's TAC of \$452,041. As ρ approaches 2 (\$690,834 for $\rho = 1.8$), TAC becomes close to that of the worst scenario, scenario 9 in Table 5.6, with TAC of \$691,383. The negligible difference between these values might have various explanations. It can happen because of the random DoE in every simulation iteration. Also, there is a possibility that the search converges to a local optimum in some cases.

If there is no ambiguity about the probability of scenarios, the nominal problem solution is the optimal. However, when there is ambiguity, uncertain parameters can randomly perturb the probabilities around their nominal values. Usually, a small value of ρ leads to a better out-of-sample performance than the stochastic solution. In this study, considering a penalty cost of \$40/kWh, the best TAC found for the robust problem is when $\rho = 0.01$, leading to a TAC of is \$470,473 with 414 PV panels, 28 wind turbines, 640 battery modules and a diesel generator with 712 kW capacity and 99% system LLP. The optimal solution achieved for $\rho = 0.01$ and \$20/kWh penalty cost is 257 PV panels, 22 wind turbines, 450 battery modules and a diesel generator with 347 kW capacity. TAC of this configuration is \$451,138 with 94.66% LLP. Optimal robust solutions achieved for different penalty costs are depicted in Table 5.9.

	Penalty cost	N_{PV}	N_{WT}	N_{bat}	Cap_{DG} (kW)	TAC	No. iteration	Time (s)	Reliability
Classical RSM	\$40/kWh	414	28	640	712	\$470,473	14	396.96	99.99%
	\$20/kWh	257	22	450	347	\$451,138	21	546.38	94.66%
	\$10/kWh	244	17	325	238	\$412,212	26	650.21	84.85%

Table 5.9: Robust problem optimal cost and configuration

In order to make sure that $\rho = 0.01$ is the actual optimum value of ρ (i.e., it did not happen by accident) and it outperforms the nominal solution ($\rho = 0$), it is necessary to perform a paired t-test for both $\rho = 0$ and $\rho = 0.01$ to determine which value of ρ (size of ambiguity set) gives a better expected out-of-sample performance and leads to a lower TAC. Therefore, the confidence interval for the difference between the two expected response, $Z = \mu_0 - \mu_{0.01}$, is constructed to determine whether the model (no jockeying) is an accurate representation of the system and whether there

is significant difference between TAC calculated with $\rho = 0$ and $\rho = 0.01$. $\mu_{0,j}$ and $\mu_{0.01,j}$ are paired together to define $Z_j = \mu_{0,j} - \mu_{0.01,j}$ for $j = 1, 2, ..., n$. Z_j are IID variables and they are normally distributed. Thus confidence interval for $E(Z_j)$ is calculated as []

$$\bar{Z}(n) = \frac{\sum_{j=1}^{n} Z_j}{n} \tag{5.2.1}$$

and

$$\hat{Var}[\bar{Z}(n)] = \frac{\sum_{j=1}^{n} [Z_j - \bar{Z}(n)]^2}{n(n-1)}. \tag{5.2.2}$$

and form the (approximate) $100(1-a)$ percent confidence interval as:

$$\bar{Z}(n) \pm t_{n-1,1-\alpha/2} \sqrt{\hat{Var}[\bar{Z}(n)]} \tag{5.2.3}$$

To asses the out-of-sample performance, 10 new random supply power realizations are generated similar to the original supply data in Section 4.1, i.e. 365 random data points are selected from both solar and wind clusters 10 times and new scenarios are used as simulation inputs.

j	$\mu_{0,j}$	$\mu_{0.01,j}$	Z_j
1	472,922	470,102	2,820
2	472,180	470,232	1,948
3	472,831	469,927	2,904
4	471,555	470,520	1,035
5	472,374	470,396	1,978
6	471,899	471,123	776
7	472,911	471,021	1,890
8	472,893	471,262	1,631
9	471,795	470,714	1,081
10	472,207	470,824	1,383

Table 5.10: TAC for 10 independent realizations with two $\rho = 0$ and $\rho = 0.01$, and their differences

TACs are calculated in Table 5.10 for \$40/kWh penalty cost and assuming normality of sample mean difference (data plot appears linear in Figure 5.6) and $\alpha =$

0.01, a paired-t test is carried out. The obtained $\bar{Z}(10) = 1744.6$ and $\hat{Var}[\bar{Z}(n)] = 51593.6$ lead to the (approximate) 90 percent confidence interval $[1328.2, 2160.9]$ for $Z = \mu_0 - \mu_{0.01}$. Thus, with approximately 90 percent confidence, it can be concluded that μ_0 differs from $\mu_{0.01}$, and it furthermore appears that $\mu_{0.01}$ is superior, since it leads to a lower TAC (between 1328.2 and 2160.9 lower).

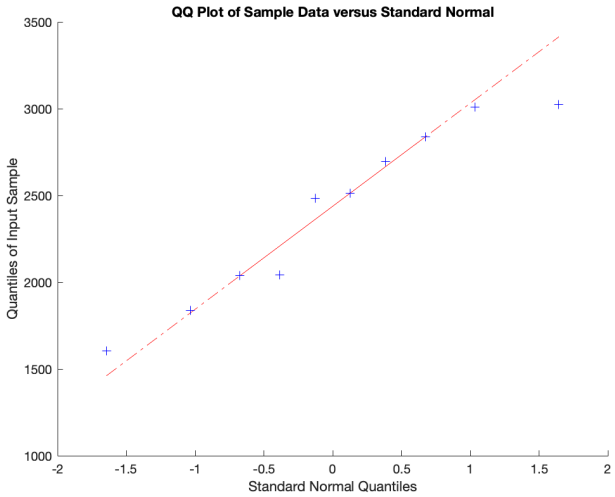

Figure 5.6: Classical RSM: QQ Plot for Z_j

The same assumption and calculations are done with new realizations for penalty costs of \$20/kWh and \$10/kWh. The calculated confidence intervals with \$20/kWh and \$10/k penalty cost for mean differences, $Z = \mu_0 - \mu_{0.01}$ are $[964.6, 1645.5]$ and $[1069.0, 1709.9]$, respectively, indicating the superiority of $\rho = 0.01$ for lowest TAC.

It is unlikely to improve one index without harming other indexes in multi-objective optimization. In general, a solution that is optimal for one objective might be (and usually is) poor for the other(s). In this study, when a high penalty cost is considered for unmet demand, the system attempts to install large number of sources and storage capacity in order to avoid shortage, which will enhance the reliability and increase the TAC. On the other extreme, by having no penalty cost, TAC can be reduced to zero by not installing any resources. However, the reliability index becomes zero, too. Therefore, the purpose is to look for "non-dominated" (or Pareto-optimal) solutions. In brief, the Pareto-optimal solution is defined as a set of "non-inferior" solutions in the objective space defining a boundary beyond which none of the objectives can be improved without sacrificing at least one of the other

objectives. Graphically, the set of nondominated solutions constitute the Pareto Frontier. The frontier in Figure 5.7 is constructed to illustrate the trade-off between TAC and reliability by changing the penalty cost and observing how the cost and reliability change. Optimal TAC derived from robust problem in Table 5.9 and their related reliability are drawn for three different penalty cost in Figure 5.10. Based on this Pareto Frontier, when a high value of penalty is considered for unmet demand, the system attempts to avoid any supply deficit and installs a large number of energy resources, which leads to high system reliability and high TAC, accordingly. As the penalty value decreases, the system allows more demand load to remain unmet since less money needs to be paid on account of supply deficiency. System reliability with \$40/kWh penalty value is 99.99% and TAC is \$470,473 and as penalty value reduces to \$10/kWh, system reliability drops below 85% and TAC reduces to \$412,212.

Figure 5.7: Classical RSM: Pareto frontier for TAC vs reliability

Based on the Pareto frontier, the decision maker decides which objective has a higher priority in system design. If a high level of system reliability is preferred, the analyst may neglect the correspondent high TAC. However, if the main objective is to reduce the TAC, the decision maker can selected the desired low TAC based on its reliability index.

5.3 GRST Results

In performing the first step of the GRST procedure, convexity of the estimated quadratic function is assured by using CVX [88] version 2.2, a Matlab-based modeling system for convex optimization. Each scenario is simulated and optimized using three different penalty costs and their optimal configuration, solution, computational time, number of iteration and reliability are illustrated in the next three tables. Tables 5.11, 5.12 and 5.13 are calculated with \$40/kWh, \$20/kWh and \$10/kWh penalty cost, respectively. It can be inferred from Table 5.11 that scenario 1, which uses cluster 1 from both the PV and wind supply power, has the lowest TAC since fewer renewable resources are needed when a high amount of power is generated. On the contrary, scenario 9, which uses cluster 3 from both PV and wind as inputs, has the highest cost due to the large number of required resources. The same conclusion can be derived from Tables 5.12 and 5.13.

Approach	Scenario # (PV#.WT#)	N_{PV}	N_{WT}	N_{bat}	Cap_{DG} (kW)	TAC	Computational Time (s)	Iteration	Reliability
GRST	1 (1.1)	122	18	278	156	\$148,720	17.25	9	100%
	2 (1.2)	290	33	460	186	\$272,907	13.57	8	100%
	3 (1.3)	330	63	792	563	\$585,298	14.54	8	99%
	4 (2.1)	154	18	390	303	\$160,030	13.69	8	100%
	5 (2.2)	214	33	373	380	\$272,029	15.33	9	100%
	6 (2.3)	518	68	680	585	\$632,415	13.65	8	99%
	7 (3.1)	252	20	255	382	\$187,639	15.42	9	100%
	8 (3.2)	218	35	340	427	\$293,317	15.11	9	100%
	9 (3.3)	466	77	664	645	\$710,267	13.64	8	100%
	10 (4.1)	263	18	278	340	\$174,194	15.17	9	100%
	11 (4.2)	395	29	587	560	\$283,589	16.11	9	99%
	12 (4.3)	227	60	590	718	\$697,880	15.26	9	100%

Table 5.11: Optimal results for each scenario with \$40/kWh penalty value

GRST terminates when the difference between the lower and upper bounds of all the variables are negligible. Therefore, the number of iterations depends on the lower and upper limit of variables. All the costs stated in $\hat{Y}^{TAC}$ column are actual costs i.e. the penalty cost is deducted from TAC in scenarios with reliability less than 100%. To hold the same initial conditions for both methods, GRST upper bound and lower

bound for each scenario are chosen based on the starting point of that scenario, i.e. the staring point of each scenario in classical RSM is within the staring range of GRST. For example, if the starting point is $[500, 40, 750, 750]$ in classical RSM, considered upper bound and lower bound for GRST are $[+20\%, +25\%, +20\%, +20\%] = [600, 50, 900, 900]$ and $[-20\%, -25\%, -20\%, -20\%] = [400, 30, 600, 600]$.

Approach	Scenario # (PV#.WT#)	N_{PV}	N_{WT}	N_{bat}	Cap_{DG} (kW)	TAC	Computational Time (s)	Iteration	Reliability
GRST	1 (1.1)	90	14	154	80	$139,478	13.73	8	94%
	2 (1.2)	214	24	363	136	$234,343	13.81	8	95%
	3 (1.3)	294	50	450	263	$562,062	12.01	7	93%
	4 (2.1)	185	14	373	56	$136,409	14.07	8	95%
	5 (2.2)	102	25	332	195	$263,084	15.82	9	95%
	6 (2.3)	293	58	383	275	$586,971	13.39	8	94%
	7 (3.1)	152	14	253	143	$176,440	15.21	9	95%
	8 (3.2)	183	25	240	168	$277,962	15.31	9	93%
	9 (3.3)	256	48	430	355	$692,291	13.44	8	94%
	10 (4.1)	131	14	205	108	$156,916	17.71	10	94%
	11 (4.2)	267	24	337	163	$271,225	15.09	9	94%
	12 (4.3)	219	42	430	342	$665,446	13.81	8	93%

Table 5.12: Optimal results for each scenario with $20/kWh penalty value

Starting with a high penalty value ($40/kWh) for unmet demand in Table 5.11 has resulted in 100% LLP for most of the scenarios since high cost must be paid as penalty for supply deficiency. Next, smaller values ($20 and $10) of the penalty per kWh are also tested and the results are presented in Tables 5.12 and 5.13. The same upper bound and lower bounds for each scenario are used for these two tables, and due to lower penalty amount, fewer number of sources are installed and accordingly, TAC has reduced while system reliability has also decreased.

Approach	Scenario # (PV#.WT#)	N_{PV}	N_{WT}	N_{bat}	Cap_{DG} (kW)	TAC	Computational Time (s)	Iteration	Reliability
GRST	1 (1.1)	66	12	86	30	$121,546	14.02	8	82%
	2 (1.2)	195	20	250	72	$218,046	15.23	9	84%
	3 (1.3)	214	39	384	205	$525,281	13.86	8	83%
	4 (2.1)	115	12	393	36	$130,449	13.77	8	84%
	5 (2.2)	93	21	302	114	$254,232	15.22	9	85%
	6 (2.3)	243	54	325	163	$539,115	13.78	8	84%
	7 (3.1)	193	12	127	60	$168,884	15.07	9	84%
	8 (3.2)	152	22	225	128	$275,682	15.48	9	86%
	9 (3.3)	215	40	310	270	$646,401	13.76	8	84%
	10 (4.1)	56	12	146	55	$148,633	15.26	9	83%
	11 (4.2)	264	20	305	106	$264,681	15.01	9	84%
	12 (4.3)	125	28	430	305	$627,092	13.35	8	85%

Table 5.13: Optimal results for each scenario with $10/kWh penalty value

To solve the nominal problem, a convex quadratic function is fit on each scenario using Equation (4.2.5) and empirical probabilities derived from clustering are used to obtain the optimal solution and configuration as in in Table 5.14 for all the three penalty costs.

	Penalty cost	N_{PV}	N_{WT}	N_{bat}	Cap_{DG} (kW)	TAC	Iteration	Computational time (s)	Reliability
GRST	$40/kWh	432	26	662	683	$472,565	11	199	99.99%
	$20/kWh	357	20	422	345	$453,499	10	209	94.46%
	$10/kWh	235	17	352	256	$414,603	11	222	85.55%

Table 5.14: Nominal problem optimal cost and configuration

Similar to the classical RSM approach, a sensitivity analysis on ρ is carried out for the second approach, GRST and is demonstrated in Figure 5.8 for three different penalty cost. For the first penalty cost, $40/kWh, like the previous method, when $\rho = 0$, there is no ambiguity and the problem is similar to the nominal (stochastic programming) problem ($472,565) with TAC of $472,893. Whereas when ρ is approaching its maximum value of 2, the TAC becomes close to the worst scenario, scenario 9 ($710,267), with TAC of $709,234 ($\rho = 1.8$). Perturbing probabilities

around their nominal values with small ρ, the best obtained TAC is with $\rho = 0.01$, which is \$471,327 with 421 PV panels, 25 wind turbines, 662 battery modules and a diesel generator with 695 kW capacity.

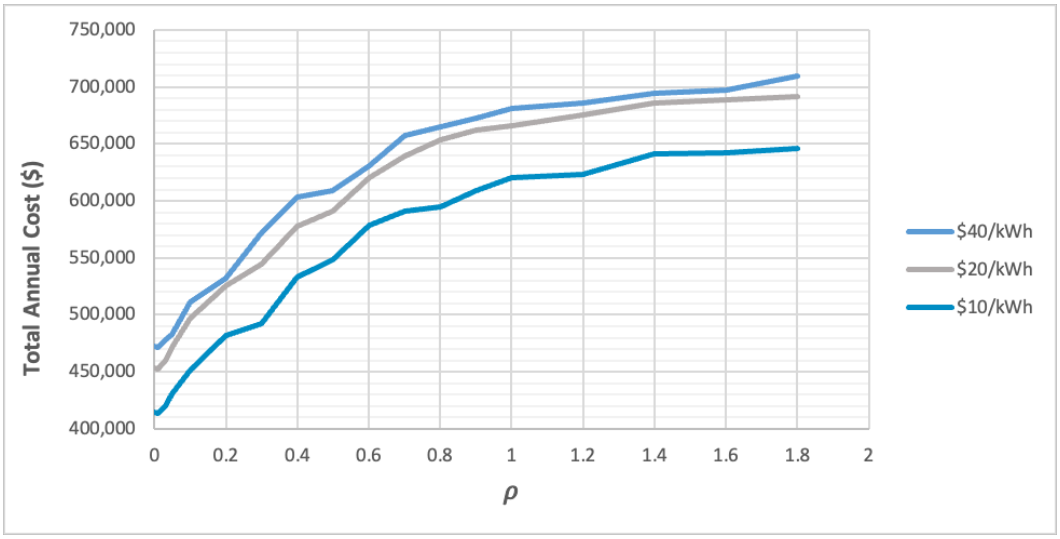

Figure 5.8: GRST: Sensitivity analysis on ρ

A similar explanation can be given regarding the solutions with \$20/kWh and \$10/kWh penalty costs. Due to their relatively lower costs, their plots situate below the solutions of \$40/kWh and as the size of the ambiguity set increases, their TAC increases too. For a \$20/kWh penalty cost, when $\rho = 0$, TAC is equal to \$453,293 (nominal problem = \$453,499) and as ρ gets closer to 2, the problem acts like the worst scenario (\$692,291) with a TAC of \$691,534 ($\rho = 1.8$). Moreover, with a penalty cost of \$10/kWh, TAC is \$414,823 and \$645,921 with $\rho = 0$ and $\rho = 1.8$, respectively. The nominal solution and the solution with $\rho = 0$ and also worst scenario solution and solution with $\rho = 2$, must coincide in theory. However, due to the random nature of GRST in every iteration for Monte Carlo simulation and the probability of approaching to local optimum, there is negligible difference (less than 0.001) between their answers. The optimal solutions found for both robust problems are with $\rho = 0.01$, which has led to the lower TAC in comparison to their nominal problem. Best solutions and configurations found for the robust problem with three different penalty costs are summarized in Table 5.15.

	Penalty cost	N_{PV}	N_{WT}	N_{bat}	Cap_{DG} (kW)	TAC	Iteration	Computational time (s)	Reliability
GRST	\$40/kWh	421	25	662	695	\$471,327	10	478	100%
	\$20/kWh	325	19	420	360	\$452,527	11	505	93.52%
	\$10/kWh	218	16	345	275	\$413,527	10	476	84.72%

Table 5.15: Robust problem optimal cost and configuration

A similar paired t-test is conducted to make sure there is significant difference between results of $\rho = 0$ and $\rho = 0.01$ and that $\rho = 0.01$ does give a better expected out-of-sample performance and leads to a lower TAC. Therefore, a confidence interval for the difference between two expected response, $Z = \mu_0 - \mu_{0.01}$, is constructed similar to the previous method and $\mu_{0,j}$ and $\mu_{0.01,j}$ are paired together to define $Z_j = \mu_{0,j} - \mu_{0.01,j}$ for n new realizations. $\bar{Z}(n)$ and $\hat{Var}[\bar{Z}(n)]$ are calculated according to Equations (5.2.1) and (5.2.2) and the (approximate) $100(1-a)$ percent confidence interval is constructed using Equation (5.2.3).

As done previously, 10 new random supply power realizations are generated similar to the original supply data and TACs are calculated in Table 5.16 with a penalty cost of \$40/kWh.

j	$\mu_{0,j}$	$\mu_{0.01,j}$	Z_j
1	473,150	471,430	1,720
2	473,926	472,665	1,261
3	473,204	472,169	1,035
4	472,810	471,576	1,234
5	473,332	472,383	949
6	472,007	471,523	484
7	472,763	471,274	1,489
8	473,075	471,551	1,524
9	471,906	471,032	874
10	472,769	471,795	974

Table 5.16: TAC for 10 independent realizations with two $\rho = 0$ and $\rho = 0.01$, and their differences

Assuming normality of the sample mean difference (data are scattered near the straight line in Figure 5.9) and $\alpha = 0.01$, a paired t-test is carried out. The obtained $\bar{Z}(10) = 1154.4$ and $\hat{Var}[\bar{Z}(n)] = 13369.5$ lead to the (approximate) 90 percent confidence interval $[942.4, 1366.3]$ for $Z = \mu_0 - \mu_{0.01}$. Thus, with approximately 90 percent confidence, it can be concluded that μ_0 differs from $\mu_{0.01}$, and it furthermore appears that $\mu_{0.01}$ is superior, since it leads to a lower TAC (between 942.4 and 1366.3 lower). The same assumption and calculation are done with new realizations for a penalty cost of \$20/kWh and \$10/kWh. The obtained confidence intervals for the mean differences, $Z = \mu_0 - \mu_{0.01}$ are $[740.1, 1489.4]$ and $[836.2, 1545.3]$ for \$20/kWh and \$10/kWh, respectively, indicating the superiority of $\rho = 0.01$ for lowest TAC.

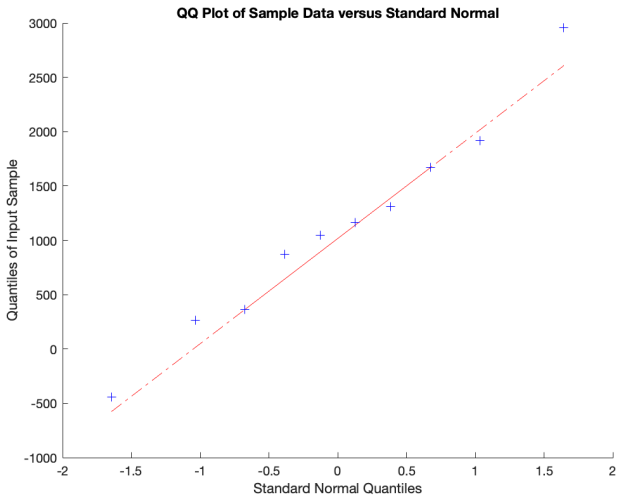

Figure 5.9: GRST: QQ Plot for Z_j

Next, a Pareto frontier is drawn to demonstrate the trade-off between TAC and reliability. As mentioned earlier, it is unlikely to improve one objective without harming other objectives in multi-objective optimization. Looking for Pareto-optimal solutions, the optimal TAC deduced from the robust problem in Table 5.15 and their corresponding LLP values are plotted for three different penalty cost values in Figure 5.10. For a high penalty value such as \$40/kWh, LLP of the system is near 100% since no unmet demand is allowed due to the high penalty price added to TAC (\$471,327). As penalty value decreases, e.g. \$20/kWh, less cost is charged in terms of unmet demand. Therefore, the system allows some demand load to remain unmet for lower TAC (\$453,127 and \$413,527) which will also results in the lower LLP

levels of 93.52% and 84.72% for $20 and $10 penalty values. From the obtained solutions, the designers can choose the penalty costs they consider more appropriate to their utility.

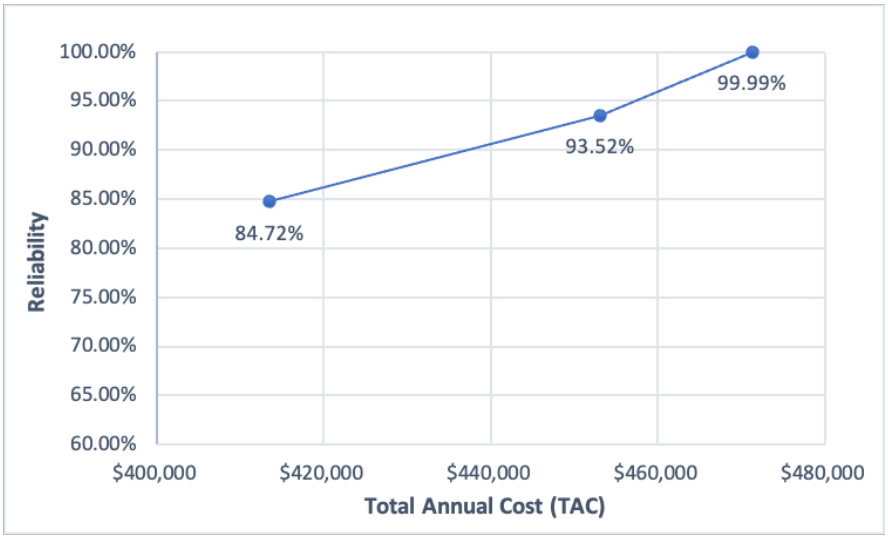

Figure 5.10: GRST: Pareto frontier for TAC vs reliability

Chapter 6

Conclusions and future extensions

Stand-alone HRES are generally more suitable than single-source systems to supply power in off-grid applications, especially in remote areas with difficult access. However, these systems must be designed carefully and account for the stochasticity and uncertainty in supply data to serve the demand at high reliability and affordable cost. In this study, a stand-alone HRES that consists of PV panels and wind turbines, integrated with battery storage and diesel generator, is considered to implement a cost-minimization design approach. In order to capture uncertainty in supply power, a finite number of scenarios with uncertain probabilities are extracted from time-series data of both solar and wind power through k-means clustering. Next, to tackle the uncertainty in scenarios' probability, an ambiguity set based on the Variation Distance phi-divergence is constructed around the nominal probability of scenarios. Since TAC and reliability functions cannot be evaluated explicitly, two novel robust simulation-optimization methods, namely Classical RSM and GRST, are proposed to estimate the objective function from a surrogate model and optimize it. Both approaches are applied on a hypothetical case study in Northwest Ontario, Canada and they show that classical RSM outperforms GRST and it leads to better solutions. The presented methods are very generic and flexible as they can be used for different applications (not only HRES design), with different objectives, operational rules, reliability metrics, scenario generation methods, ambiguity sets, etc.

The Classical RSM first investigates the neighborhood of the starting point by fitting a first-order polynomial and moves towards the optimal solution in the steepest descent direction. Then, it fits a second-order polynomial on the neighborhood of the last-reached solution. In GRST, a second-order polynomial is fit on the entire feasible area from the beginning, then search regions are restricted around the latest found optimal solution. Therefore, there is a high chance that the problem does

not converge to a global optimum and instead gets stuck in a local optimum. The classical RSM is highly dependents on the starting points and design variables' levels, i.e., R-III and CCD levels and intervals. CCDs are rather inefficient because they use inefficient resolution-V designs and add 2k axial points and five values per factor result. If the better outputs seem to lie in the certain corner of Figure 4.2, then it is efficient to simulate only the two points $(-c, 0)'$ and $(0, -c)'$ for a better estimation of the second-order polynomial [76]. To reach the optimal solution with the classical RSM, the analyst must have a prior knowledge regarding the system. On the other hand, GRST is an easy-to-implement method which gives a relatively good answer in a short time.

Using classical RSM, the optimal solutions found for the nominal problem with all the three penalty values lead to lower TAC values in comparison to second approach, GRST. Running a sensitivity analysis on ρ for both methods in the robust problem, the size of ambiguity set with $\rho = 0.01$ leads to a lower TAC in comparison to the nominal problem, and conducting a paired t-test proves the same outcome for out-of-sample performance. Regarding all numerical outcomes, classical RSM has led to better optimal solution and reliability in comparison to GRST, while the GRST computational time is relatively shorter than classical RSM. However the results from the two approaches are not statistically different for various penalty values and their difference is less than 0.5%. In the end, a Pareto frontier is depicted for both methods to illustrate the trade-off between TAC as a results of different penalty values and the level of system reliability. According to the frontiers, as the higher reliability index is expected from HRES, higher amount of TAC needs to be paid in order to satisfy the expectation. On the contrary, if the analyst prefers a less expensive HRES (lower TAC), they shall accept a reduction in system reliability. To verify the simulation, the optimal input combinations obtained from the metamodels are checked and compared with the simulation model output, and insignificant differences (less than 1%) between both outputs are found.

For future studies, other sources of renewable energy such as biomass, hydro, etc. can be used alongside / instead of PV/wind/battery/diesel system in order to build a robust and reliable energy system. Moreover, other objectives like minimizing GHG emissions and minimizing energy losses can be considered alongside cost

minimization and reliability maximization. Also, alternative metamodel-based approaches for simulation optimization similar to Kriging and neural network can be implemented to estimate the objective function as a surrogate model. Finally, other types of phi-divergence such as Kullback-Leibler, χ^2 distance, can be utilized to construct the ambiguity set and compared with the currently-used Variation Distance phi-divergence.

Bibliography

[1] R. Banos, F. Manzano-Agugliaro, F. Montoya, C. Gil, A. Alcayde, and J. Gómez, "Optimization methods applied to renewable and sustainable energy: A review," *Renewable and sustainable energy reviews*, vol. 15, no. 4, pp. 1753–1766, 2011.

[2] Y. Sawle, S. Gupta, and A. K. Bohre, "Review of hybrid renewable energy systems with comparative analysis of off-grid hybrid system," *Renewable and Sustainable Energy Reviews*, vol. 81, pp. 2217–2235, 2018.

[3] R. Siddaiah and R. Saini, "A review on planning, configurations, modeling and optimization techniques of hybrid renewable energy systems for off grid applications," *Renewable and Sustainable Energy Reviews*, vol. 58, pp. 376–396, 2016.

[4] M. Amer, A. Namaane, and N. M'sirdi, "Optimization of hybrid renewable energy systems using pso for cost reduction," *Energy Procedia*, vol. 42, pp. 318–327, 2013.

[5] J. L. Bernal-Agustín, R. Dufo-López, and D. M. Rivas-Ascaso, "Design of isolated hybrid systems minimizing costs and pollutant emissions," *Renewable Energy*, vol. 31, no. 14, pp. 2227–2244, 2006.

[6] B. O. Bilal, V. Sambou, C. Kébé, P. Ndiaye, and M. Ndongo, "Methodology to size an optimal stand-alone pv/wind/diesel/battery system minimizing the levelized cost of energy and the co2 emissions," *Energy Procedia*, vol. 14, pp. 1636–1647, 2012.

[7] A. Billionnet, M.-C. Costa, and P.-L. Poirion, "Robust optimal sizing of a hybrid energy stand-alone system," *European Journal of Operational Research*, vol. 254, no. 2, pp. 565–575, 2016.

[8] P. Nema, R. Nema, and S. Rangnekar, "Minimization of green house gases emission by using hybrid energy system for telephony base station site application," *Renewable and Sustainable Energy Reviews*, vol. 14, no. 6, pp. 1635–1639, 2010.

[9] S. Klein and W. Beckman, "Loss-of-load probabilities for stand-alone photovoltaic systems," *Solar Energy*, vol. 39, no. 6, pp. 499–512, 1987.

[10] E. Ofry and A. Braunstein, "The loss of power supply probability as a technique for designing stand-alone solar electrical (photovoltaic) systems," *IEEE Transactions on Power Apparatus and Systems*, no. 5, pp. 1171–1175, 1983.

[11] R. Ramakumar, P. S. Shetty, and K. Ashenayi, "A linear programming approach to the design of integrated renewable energy systems for developing countries," *IEEE Transactions on Energy Conversion*, no. 4, pp. 18–24, 1986.

[12] S. Shaahid and M. Elhadidy, "Prospects of autonomous/stand-alone hybrid (photo-voltaic+ diesel+ battery) power systems in commercial applications in hot regions," *Renewable energy*, vol. 29, no. 2, pp. 165–177, 2004.

[13] D. Xu, L. Kang, L. Chang, and B. Cao, "Optimal sizing of standalone hybrid wind/pv power systems using genetic algorithms," in *Canadian Conference on Electrical and Computer Engineering, 2005.*, pp. 1722–1725, IEEE, 2005.

[14] H. Yang, Z. Wei, and L. Chengzhi, "Optimal design and techno-economic analysis of a hybrid solar–wind power generation system," *Applied energy*, vol. 86, no. 2, pp. 163–169, 2009.

[15] M. Deshmukh and S. Deshmukh, "Modeling of hybrid renewable energy systems," *Renewable and sustainable energy reviews*, vol. 12, no. 1, pp. 235–249, 2008.

[16] B. Y. Ekren and O. Ekren, "Simulation based size optimization of a pv/wind hybrid energy conversion system with battery storage under various load and auxiliary energy conditions," *Applied Energy*, vol. 86, no. 9, pp. 1387–1394, 2009.

[17] O. Ekren and B. Y. Ekren, "Size optimization of a pv/wind hybrid energy conversion system with battery storage using response surface methodology," *Applied energy*, vol. 85, no. 11, pp. 1086–1101, 2008.

[18] M. S. Ismail, M. Moghavvemi, and T. Mahlia, "Genetic algorithm based optimization on modeling and design of hybrid renewable energy systems," *Energy Conversion and Management*, vol. 85, pp. 120–130, 2014.

[19] K. Zou, A. Agalgaonkar, K. M. Muttaqi, and S. Perera, "Voltage support by distributed generation units and shunt capacitors in distribution systems," in *2009 IEEE Power & Energy Society General Meeting*, pp. 1–8, IEEE, 2009.

[20] A. Askarzadeh and L. dos Santos Coelho, "A novel framework for optimization of a grid independent hybrid renewable energy system: A case study of iran," *Solar Energy*, vol. 112, pp. 383–396, 2015.

[21] A. Maheri, "Multi-objective design optimisation of standalone hybrid wind-pv-diesel systems under uncertainties," *Renewable Energy*, vol. 66, pp. 650–661, 2014.

[22] J. Ahmad, M. Imran, A. Khalid, W. Iqbal, S. R. Ashraf, M. Adnan, S. F. Ali, and K. S. Khokhar, "Techno economic analysis of a wind-photovoltaic-biomass hybrid renewable energy system for rural electrification: A case study of kallar kahar," *Energy*, vol. 148, pp. 208–234, 2018.

[23] Y. Carson and A. Maria, "Simulation optimization: methods and applications," in *Proceedings of the 29th conference on Winter simulation*, pp. 118–126, 1997.

[24] H. Energy, "Hybrid optimization of multiple energy resources." `https://www.homerenergy.com/`, 2020.

[25] I. . MHOGA, "Simulation and optimization of stand-alone and grid-connected hybrid renewable systems." `https://ihoga.unizar.es/`, 2020.

[26] OptTek, "Optquest the world's leading simulation optimization engine." `https://www.opttek.com/products/optquest/`, 2020.

[27] A. González, J.-R. Riba, and A. Rius, "Optimal sizing of a hybrid grid-connected photovoltaic–wind–biomass power system," *Sustainability*, vol. 7, no. 9, pp. 12787–12806, 2015.

[28] S. Twaha and M. A. Ramli, "A review of optimization approaches for hybrid distributed energy generation systems: Off-grid and grid-connected systems," *Sustainable Cities and Society*, vol. 41, pp. 320–331, 2018.

[29] C. L. Borges and D. M. Falcao, "Optimal distributed generation allocation for reliability, losses, and voltage improvement," *International Journal of Electrical Power & Energy Systems*, vol. 28, no. 6, pp. 413–420, 2006.

[30] M. B. Shadmand and R. S. Balog, "Multi-objective optimization and design of photovoltaic-wind hybrid system for community smart dc microgrid," *IEEE Transactions on Smart Grid*, vol. 5, no. 5, pp. 2635–2643, 2014.

[31] D. Abbes, A. Martinez, and G. Champenois, "Life cycle cost, embodied energy and loss of power supply probability for the optimal design of hybrid power systems," *Mathematics and Computers in Simulation*, vol. 98, pp. 46–62, 2014.

[32] R. Dufo-López and J. L. Bernal-Agustín, "Design and control strategies of pv-diesel systems using genetic algorithms," *Solar energy*, vol. 79, no. 1, pp. 33–46, 2005.

[33] R. Dufo-López, J. L. Bernal-Agustín, J. Lujano, and J. A. Domínguez-Navarro, "Utilization of synthetically generated hourly wind speed data in the optimization of wind-batteries stand-alone systems," in *Proc. 2011 International Conference on Renewable Energies and Power Quality¡ http://www. icrepq. com/icrepq*, vol. 2711, 2011.

[34] A. Saif, V. R. Pandi, H. Zeineldin, and S. Kennedy, "Optimal allocation of distributed energy resources through simulation-based optimization," *Electric Power Systems Research*, vol. 104, pp. 1–8, 2013.

[35] S. Upadhyay and M. Sharma, "Development of hybrid energy system with cycle charging strategy using particle swarm optimization for a remote area in india," *Renewable Energy*, vol. 77, pp. 586–598, 2015.

[36] H. Baghaee, M. Mirsalim, G. Gharehpetian, and H. Talebi, "Reliability/cost-based multi-objective pareto optimal design of stand-alone wind/pv/fc generation microgrid system," *Energy*, vol. 115, pp. 1022–1041, 2016.

[37] M. Sharafi and T. Y. ElMekkawy, "Stochastic optimization of hybrid renewable energy systems using sampling average method," *Renewable and Sustainable Energy Reviews*, vol. 52, pp. 1668–1679, 2015.

[38] O. Ekren and B. Y. Ekren, "Size optimization of a pv/wind hybrid energy conversion system with battery storage using simulated annealing," *Applied energy*, vol. 87, no. 2, pp. 592–598, 2010.

[39] S. Singh and S. C. Kaushik, "Optimal sizing of grid integrated hybrid pv-biomass energy system using artificial bee colony algorithm," *IET Renewable Power Generation*, vol. 10, no. 5, pp. 642–650, 2016.

[40] S. Singh, M. Singh, and S. C. Kaushik, "Feasibility study of an islanded microgrid in rural area consisting of pv, wind, biomass and battery energy storage system," *Energy Conversion and Management*, vol. 128, pp. 178–190, 2016.

[41] X. Pelet, D. Favrat, and G. Leyland, "Multiobjective optimisation of integrated energy systems for remote communities considering economics and co2 emissions," *International journal of Thermal sciences*, vol. 44, no. 12, pp. 1180–1189, 2005.

[42] E. Angün, J. Kleijnen, D. den Hertog, and G. Gürkan, "Response surface methodology with stochastic constraints for expensive simulation," *Journal of the operational research society*, vol. 60, no. 6, pp. 735–746, 2009.

[43] A. Kanase-Patil, R. Saini, and M. Sharma, "Integrated renewable energy systems for off grid rural electrification of remote area," *Renewable Energy*, vol. 35, no. 6, pp. 1342–1349, 2010.

[44] P. Malik, M. Awasthi, and S. Sinha, "Study of grid integrated biomass-based hybrid renewable energy systems for himalayan terrain," *International Journal of Sustainable Energy Planning and Management*, vol. 28, pp. 71–88, 2020.

[45] S. Bentouba and M. Bourouis, "Feasibility study of a wind–photovoltaic hybrid power generation system for a remote area in the extreme south of algeria," *Applied Thermal Engineering*, vol. 99, pp. 713–719, 2016.

[46] P. Balamurugan, S. Ashok, and T. Jose, "Optimal operation of biomass/wind/pv hybrid energy system for rural areas," *International Journal of Green Energy*, vol. 6, no. 1, pp. 104–116, 2009.

[47] R. R. Barton, "Simulation optimization using metamodels," in *Proceedings of the 2009 winter simulation conference (WSC)*, pp. 230–238, IEEE, 2009.

[48] Y. Ohsawa, S.-i. Emura, and K. Arai, "Optimal operation of photovoltaic/diesel power generation system by neural network," in *[1993] Proceedings of the Second International Forum on Applications of Neural Networks to Power Systems*, pp. 99–103, IEEE, 1992.

[49] A. Mellit, M. Benghanem, A. H. Arab, and A. Guessoum, "An adaptive artificial neural network model for sizing stand-alone photovoltaic systems: application for isolated sites in algeria," *Renewable energy*, vol. 30, no. 10, pp. 1501–1524, 2005.

[50] A. Mellit, S. A. Kalogirou, and M. Drif, "Application of neural networks and genetic algorithms for sizing of photovoltaic systems," *Renewable Energy*, vol. 35, no. 12, pp. 2881–2893, 2010.

[51] O. Ekren, B. Y. Ekren, and B. Ozerdem, "Break-even analysis and size optimization of a pv/wind hybrid energy conversion system with battery storage–a case study," *Applied Energy*, vol. 86, no. 7-8, pp. 1043–1054, 2009.

[52] H. Ren, Z. Ma, W. Li, V. Tyagi, and A. Pandey, "Optimisation of a renewable cooling and heating system using an integer-based genetic algorithm, response surface method and life cycle analysis," *Energy Conversion and Management*, vol. 230, p. 113797, 2021.

[53] K.-H. Chang and G. Lin, "Optimal design of hybrid renewable energy systems using simulation optimization," *Simulation Modelling Practice and Theory*, vol. 52, pp. 40–51, 2015.

[54] A. Sóbester, S. J. Leary, and A. J. Keane, "On the design of optimization strategies based on global response surface approximation models," *Journal of Global Optimization*, vol. 33, no. 1, pp. 31–59, 2005.

[55] M. Rais-Rohani and M. Singh, "Comparison of global and local response surface techniques in reliability-based optimization of composite structures," *Structural and Multidisciplinary Optimization*, vol. 26, no. 5, pp. 333–345, 2004.

[56] G. Dellino, J. P. Kleijnen, and C. Meloni, "Robust optimization in simulation: Taguchi and response surface methodology," *International Journal of Production Economics*, vol. 125, no. 1, pp. 52–59, 2010.

[57] G. Dellino, J. P. Kleijnen, and C. Meloni, "Metamodel-based robust simulation-optimization: An overview," in *Uncertainty Management in Simulation-Optimization of Complex Systems*, pp. 27–54, Springer, 2015.

[58] G. Dellino, J. P. Kleijnen, and C. Meloni, "Parametric and distribution-free bootstrapping in robust simulation-optimization," in *Proceedings of the 2010 Winter Simulation Conference*, pp. 1283–1294, IEEE, 2010.

[59] G. Dellino, J. P. Kleijnen, and C. Meloni, "Robust optimization in simulation: Taguchi and krige combined," *INFORMS Journal on Computing*, vol. 24, no. 3, pp. 471–484, 2012.

[60] L. X Andy Sun, "Robust optimization in electric power systems operations," *Springer International Publishing*, pp. 227–258, 2017.

[61] T. Dragičević, H. Pandžić, D. Škrlec, I. Kuzle, J. M. Guerrero, and D. S. Kirschen, "Capacity optimization of renewable energy sources and battery storage in an autonomous telecommunication facility," *IEEE Transactions on Sustainable Energy*, vol. 5, no. 4, pp. 1367–1378, 2014.

[62] E. Delage and Y. Ye, "Distributionally robust optimization under moment uncertainty with application to data-driven problems," *Operations research*, vol. 58, no. 3, pp. 595–612, 2010.

[63] F. Alismail, P. Xiong, and C. Singh, "Optimal wind farm allocation in multi-area power systems using distributionally robust optimization approach," *IEEE Transactions on Power Systems*, vol. 33, no. 1, pp. 536–544, 2017.

[64] A. Ben-Tal, D. Den Hertog, A. De Waegenaere, B. Melenberg, and G. Rennen, "Robust solutions of optimization problems affected by uncertain probabilities," *Management Science*, vol. 59, no. 2, pp. 341–357, 2013.

[65] L. Pardo, *Statistical inference based on divergence measures*. CRC press, 2018.

[66] S. Moghaddam and M. Mahlooji, "Robust simulation optimization using φ-divergence," *International Journal of Industrial Engineering Computations*, vol. 7, no. 4, pp. 517–534, 2016.

[67] Z. Wang, P. W. Glynn, and Y. Ye, "Likelihood robust optimization for data-driven problems," *Computational Management Science*, vol. 13, no. 2, pp. 241–261, 2016.

[68] D. Klabjan, D. Simchi-Levi, and M. Song, "Robust stochastic lot-sizing by means of histograms," *Production and Operations Management*, vol. 22, no. 3, pp. 691–710, 2013.

[69] G. C. Calafiore, "Ambiguous risk measures and optimal robust portfolios," *SIAM Journal on Optimization*, vol. 18, no. 3, pp. 853–877, 2007.

[70] C. D. Barley and C. B. Winn, "Optimal dispatch strategy in remote hybrid power systems," *Solar Energy*, vol. 58, no. 4-6, pp. 165–179, 1996.

[71] J. L. Bernal-Agustín and R. Dufo-Lopez, "Simulation and optimization of stand-alone hybrid renewable energy systems," *Renewable and sustainable energy reviews*, vol. 13, no. 8, pp. 2111–2118, 2009.

[72] S. Miyamoto, H. Ichihashi, K. Honda, and H. Ichihashi, *Algorithms for fuzzy clustering*. Springer, 2008.

[73] G. Bayraksan and D. K. Love, "Data-driven stochastic programming using phi-divergences," in *The Operations Research Revolution*, pp. 1–19, INFORMS, 2015.

[74] H. Rahimian, G. Bayraksan, and T. Homem-de Mello, "Identifying effective scenarios in distributionally robust stochastic programs with total variation distance," *Mathematical Programming*, vol. 173, no. 1, pp. 393–430, 2019.

[75] G. E. Box and K. B. Wilson, "On the experimental attainment of optimum conditions," *Journal of the royal statistical society: Series b (Methodological)*, vol. 13, no. 1, pp. 1–38, 1951.

[76] J. P. Kleijnen, "Design and analysis of simulation experiments," in *International Workshop on Simulation*, pp. 3–22, Springer, 2015.

[77] J. P. Kleijnen, D. Den Hertog, and E. Angün, "Response surface methodology's steepest ascent and step size revisited," *European Journal of Operational Research*, vol. 159, no. 1, pp. 121–131, 2004.

[78] J. P. Kleijnen, "Response surface methodology for constrained simulation optimization: An overview," *Simulation Modelling Practice and Theory*, vol. 16, no. 1, pp. 50–64, 2008.

[79] M. Bashiri and F. Samaei, "Heuristic and metaheuristic structure of response surface methodology in process optimization," in *2011 IEEE International Conference on Industrial Engineering and Engineering Management*, pp. 1495–1499, IEEE, 2011.

[80] J. P. Kleijnen, "Simulation and optimization in production planning: a case study," *Decision Support Systems*, vol. 9, no. 3, pp. 269–280, 1993.

[81] D. R. Jones, "A taxonomy of global optimization methods based on response surfaces," *Journal of global optimization*, vol. 21, no. 4, pp. 345–383, 2001.

[82] I. E. S. Operator, "Data directory." `http://www.ieso.ca/en/Power-Data/Data-Directory`, 2020.

[83] T. I. E. S. O. (IESO), "Generator output and capability." `http://reports.ieso.ca/public/GenOutputCapability/`, 2021.

[84] N. Insulators, "Structure of nas energy storage system." `https://www.ngk-insulators.com/en/product/nas-configurations.html`, 2021.

[85] unplugged Power Systems, "Atlantic canada's leader in alternative energy.." `https://unpluggedpowersystems.ca/`, 2021.

[86] M. Yazdani, M. Salam, and Q. Rahman, "Investigation of the effect of weather conditions on solar radiation in brunei darussalam," *International Journal of Sustainable Energy*, vol. 35, no. 10, pp. 982–995, 2016.

[87] G. Optimization, "Linear programming (lp) – a primer on the basics." `https://www.gurobi.com/resource/linear-programming-basics/`, 2021.

[88] C. Research, "Cvx: Matlab software for disciplined convex programming." `http://cvxr.com/cvx/`, 2012.